iScience

CellPress
OPEN ACCESS

Article

Platelet-derived growth factor receptor beta is required for embryonic specification and confinement of the adult white adipose lineage

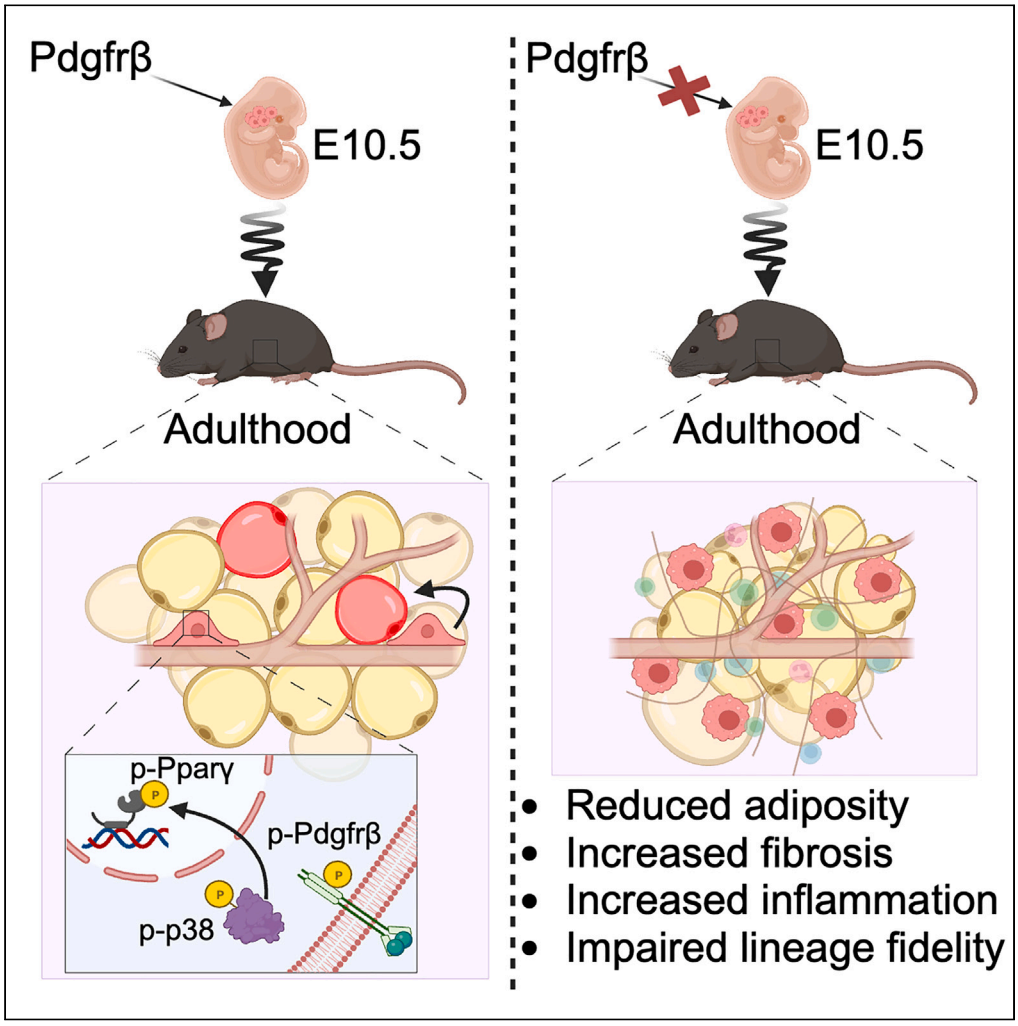

Abigail M. Benvie, Derek Lee, Yuwei Jiang, Daniel C. Berry

dcb37@cornell.edu

Highlights

Pdgfrβ deletion results in adult-onset white adipose tissue dysfunction

Pdgfrβ is required for adult adipose lineage confinement and adult adipogenesis

Embryonic deletion of Pdgfrβ results in adipocyte-to-macrophage lineage conversion

Pdgfrβ signaling upholds the APC state but halts adipogenesis by Pparγ^{Ser112}

Benvie et al., iScience 27, 108682
January 19, 2024
https://doi.org/10.1016/j.isci.2023.108682

iScience

CellPress
OPEN ACCESS

Article

Platelet-derived growth factor receptor beta is required for embryonic specification and confinement of the adult white adipose lineage

Abigail M. Benvie,[1] Derek Lee,[1] Yuwei Jiang,[2] and Daniel C. Berry[1,3,*]

SUMMARY

White adipose tissue (WAT) development and adult homeostasis rely on distinct adipocyte progenitor cells (APCs). While adult APCs are defined early during embryogenesis and generate adipocytes after WAT organogenesis, the mechanisms underlying adult adipose lineage determination and preservation remain undefined. Here, we uncover a critical role for platelet-derived growth factor receptor beta (Pdgfrβ) in identifying the adult APC lineage. Without Pdgfrβ, APCs lose their adipogenic competency to incite fibrotic tissue replacement and inflammation. Through lineage tracing analysis, we reveal that the adult APC lineage is lost and develops into macrophages when Pdgfrβ is deleted embryonically. Moreover, to maintain the APC lineage, Pdgfrβ activation stimulates p38/MAPK phosphorylation to promote APC proliferation and maintains the APC state by phosphorylating peroxisome proliferator activated receptor gamma (Pparγ) at serine 112. Together, our findings identify a role for Pdgfrβ acting as a rheostat for adult adipose lineage confinement to prevent unintended lineage switches.

INTRODUCTION

White adipose tissues (WATs) are specified and formed embryonically and during the peripartum period and are maintained throughout life.[1,2] During development, WAT depots are separated into subcutaneous and visceral compartments, which appear to have distinct lineages and metabolic functions.[3–5] Nevertheless, once generated, white adipocytes store excess nutrients as triglycerides and regulate glucose and lipid metabolism, control hunger, provide reproductive cues, and perform thermogenesis under environmental stress.[6] Accordingly, maintaining proper WAT function is critical for preserving metabolic health, as too much (obesity) or too little (lipodystrophy) can accelerate metabolic disease.[7] A key feature of WAT health is the ability to produce new adipocytes to regulate tissue turnover and renewal, depending on nutrient load and homeostatic cues.[8] Yet, chronic overnutrition can disrupt this balance by stimulating triglyceride synthesis in existing adipocytes—hypertrophy. Additionally, recent evidence suggests that obesity can prompt new adipocyte formation, suggesting an adipocyte progenitor cell (APC) compartment.[9]

For most organs, such as blood, gut, and skeletal muscle, stem or progenitor cell pools are required for tissue development, homeostasis, and regeneration. Indeed, genetic fate mapping approaches, prospective flow cytometric studies, and single-cell transcriptomics have revealed APC pools residing within WATs that can form adipocytes under homeostatic and obesogenic conditions.[10–17] For instance, we have begun to characterize a pool of committed APCs that express the critical regulator of adipogenesis, peroxisome proliferator-activated receptor gamma (Pparγ).[14,15] Using a Pparγ adipose tissue genetic fate mapping tool, AdipoTrak, we have shown that AdipoTrak-marked APCs can generate adipocytes during WAT development and adult homeostasis.[14] Briefly, AdipoTrak is a doxycycline-inducible system that incorporates a Pparγ-tTA knocked into the endogenous locus of Pparγ combined with the dynamic TRE-H2B-GFP and the indelible Rosa26^{tdTomato} reporters to mark and track APCs.[15] Of note, AdipoTrak mice are heterozygous for Pparγ. Nevertheless, genetic necessity and sufficiency tests have demonstrated the essentiality of AdipoTrak-labeled APCs in generating and maintaining WAT depots.[14] Yet, how the Pparγ-marked adipose lineage is determined and maintained has yet to be explored.

Typically, tissue-resident precursor cells reside in specialized microenvironments, the niche, which can regulate progenitor cell biology and function.[18] Corresponding to this notion, adult AdipoTrak-APCs reside in a vascular niche along the vascular wall, express several mural cell markers, and display mural cell characteristics.[14,19] Intriguingly, the APCs that develop the WAT organ do not reside in a vascular niche nor resemble smooth muscle cells rather they appear distinct but do commonly express Pparγ.[14,20] Changes in APC niches and their requirements for WAT organogenesis versus homeostasis suggested distinct progenitor cell lineages that develop and maintain the tissues. In agreement, embryonic lineage studies examining Pparγ expression, showed that adult APCs are expressed early during embryogenesis—embryonic day (E) 10.5 (E10.5). However, these cells only infiltrate and acquire tissue residency after embryonic WAT development, around postnatal day (P)

[1]Division of Nutritional Sciences, Cornell University, Ithaca, NY 14853, USA
[2]Department of Physiology and Biophysics, University of Illinois College of Medicine at Chicago, Chicago, IL 60612, USA
[3]Lead contact
*Correspondence: dcb37@cornell.edu
https://doi.org/10.1016/j.isci.2023.108682

30 (P30).[14] In agreement, Pref-1, an APC hallmark, genetic studies revealed an E10.5 labeled progenitor capable of forming adipocytes, suggesting an early mesodermal origin of WAT.[21] Even more intriguing is the requirement of the APC niche in arbitering adipogenic cues. For instance, platelet-derived growth factor receptor beta (Pdgfrβ) facilitates APC-niche interaction to coordinate WAT vascular expansion and *in vivo* adipogenesis. Specifically, deleting Pdgfrβ results in APC mislocalization, while Pdgfrβ constitutive activation can lock APCs within the vascular niche. What's more is that Pparγ appears to direct APC niche presence and expansion by transcriptionally regulating Pdgfrβ and vascular endothelial growth factor (Vegf).[19] Nevertheless, several interesting questions arose from these studies, for instance, what are the required molecular mechanisms for *adult* APC lineage commitment, confinement, and stemness that coordinate *adult* APC WAT homeostasis and expansion?

Here, we show that in addition to niche residency, Pdgfrβ functions as a molecular regulator to specify the adult adipose lineage to direct adult WAT homeostasis. Deleting Pdgfrβ throughout the adipose lineage renders APCs non-adipogenic, resulting in fibrotic tissue replacement and immune cell infiltration. Using indelible lineage tracing techniques, we observed that Pdgfrβ deficient adult APCs had undergone a fate change to resemble macrophages. Mechanistically, we find that Pdgfrβ via p38/Mapk signaling controls APC lineage expansion and avoids adipogenesis by Pparγ phosphorylation. Collectively, our data suggest that Pdgfrβ is critical for APC lineage decisions and specification, allowing for proper adult WAT homeostasis and expansion.

RESULTS

Embryonic-derived adipocyte progenitor cells occupy niches and generate adipocytes in the adult white adipose tissue

Adult APCs are specified at E10.5 but occupy WAT depots after tissue organogenesis. Upon entry, adult APCs reside along blood vessel walls, resemble mural cells, and can generate new adipocytes.[14] Pursing this progression, we evaluated doxycycline-suppressed E10.5-labeled AdipoTrak (*Pparγ-tTA*; *TRE-Cre*; *Rosa26-lox-stop-lox-tdTomato* (*R26R*$^{tdTomato/+}$)) APCs at various WAT developmental and adult time points for entry and niche residency (Figure 1A). We found that at P10, a developmental timepoint, AdipoTrak$^{-tdTomato}$ signal was undetectable, as previously observed.[14] In contrast, by P30, the completion of WAT organogenesis, we could observe the tdTomato signal along the WAT vasculature (Figures 1B and S1A). In agreement with the notion that these cells just arrived, only rare adipocyte labeling could be observed. However, with age (P60 and P120), we could identify vasculature and adipocyte labeling demonstrating their adipogenic propensity and WAT homeostatic response (Figures 1B and S1A). Of note, changes in cellular labeling were not attributed to alterations in Dox diet intake (Figure S1B). In agreement, image quantification of tdTomato-positive adipocytes demonstrated increased adipocyte labeling between P60 and P120, suggesting continued adipocyte generation with age (Figure S1C). To evaluate adult APC tissue entry and vascular occupancy, we took advantage of an organotypic native niche assay that isolates tiny blood vessel fragments called stromal vascular particulates (SVPs) from inguinal WAT (iWAT) depots.[15] Notably, SVPs isolated from P10 WAT depots were void of tdTomato signal. In contrast, at P- 30, 60, and 90, we could observe the vascular presence of E10.5 AdipoTrak-labeled adult APCs, suggesting that these cells occupy WAT niche positions after tissue development (Figures 1C and S1D). We also assessed if E10.5 AdipoTrak-labeled cells were restricted to the adipose lineage. By flow cytometric analysis, we did not observe an overlap with hematopoietic (CD45) or endothelial (CD31) lineages (Figures S1E and S1F). To confirm the adipogenic potential of E10.5 AdipoTrak-labeled cells, we performed *in vitro* adipogenic assessment on stromal vasculature (SV) cultures from E10.5 Dox-suppressed mice. We found that most adipocytes emanated from E10.5-labeled cells, suggesting that these cells are functional APCs (Figures S1G–S1I).

Platelet-derived growth factor receptor beta function is critical for white adipose tissue homeostasis and maintenance

To explore relevant mechanisms for adult APC WAT niche infiltration, we exploited the notion that Pdgfrβ regulates APC niche occupancy and WAT expansion.[19] Toward this end, we combined the Pdgfrβ$^{fl/fl}$ conditional mouse model with the AdipoTrak (*Pparγ-tTA*; *TRE-Cre*; *TRE-H2B-GFP*) (Pdgfrβ^{AT}KO) system and evaluated non-Dox suppressed control and mutant mice at P-10, 30, 60, and 120 (Figure 2A). In this model, we combined the AdipoTrak system with the TRE-H2B-GFP (H2B, Histone 2B) reporter to monitor APC abundance and cellular fate.[22] Evaluation of control and mutant mice P10 and P30 revealed comparable adipose tissue (subcutaneous and visceral) weights and morphology (Figures 2B–2D and S2A). However, at P60 and P120, we observed less adiposity and disordered adipose tissue architecture in Pdgfrβ mutant mice compared to controls (Figures 2B–2D and S2A). To examine vascular niche residency between control and mutant mice, we evaluated SVPs for AdipoTrak-GFP cell occupancy and density. Comparable to the E10.5 lineage tracing studies, the GFP signal along SVPs from P10 iWAT samples was undetectable. Yet, at P-30, -60, and −90, control SVPs demonstrated GFP-positive cells along blood vessel fragments. In contrast, Pdgfrβ^{AT}KO mutants showed limited APC presence along SVPs suggesting impaired progenitor-vascular niche interaction, in agreement with our previous findings (Figures 2E and S2B).

Because we observed robust differences at P60, we continued to evaluate this time point. Nuclear magnetic resonance (NMR) body composition analysis revealed a 50% reduction in body fat content (Figure S2C). In agreement with less adiposity, serum adiponectin—an adipokine that correlates with adipose tissue health—levels were significantly reduced in Pdgfrβ^{AT}KO mice compared to controls (Figure S2D). In agreement with WAT weight, the visual inspection of mutant subcutaneous and visceral WAT revealed significantly smaller depots than controls (Figure S2E). Quantifying adipocyte size from hematoxylin and eosin (H&E) images revealed that the remaining adipocytes were hypertrophied in iWAT and perigonadal WAT (gWAT) under a normal chow diet (NCD) (Figure S2F). The lack of adipose tissue mass suggested a defect in progenitor adipogenic competency. Indeed, *in vitro* adipogenesis revealed that Pdgfrβ-deficient APCs were non-adipogenic compared to control APCs (Figures S2G and S2H).

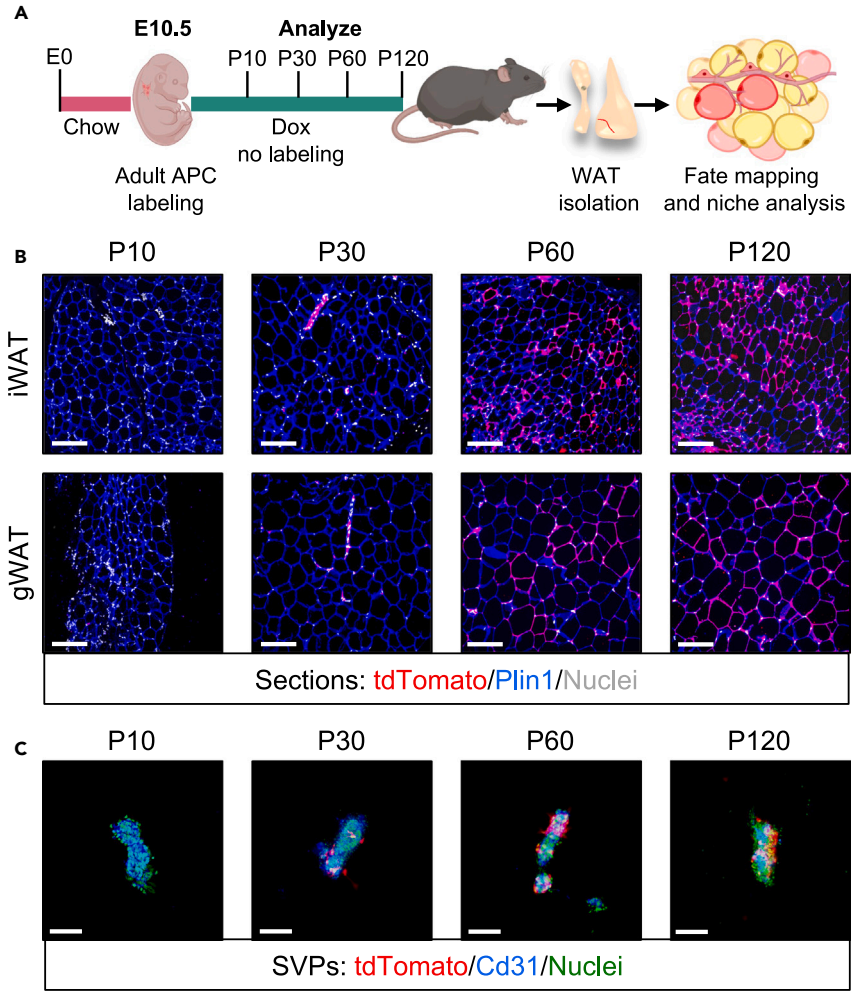

Figure 1. Embryonically derived APCs occupy vascular niches and generate adipocytes in adult WAT

(A) Experimental design: Control^{AT} (Pparγ-tTA; TRE-Cre; R26R^{tdtomato}) APCs are labeled prior to E10.5. At E10.5 pregnant dams were administered a doxycycline (Dox) diet. AdipoTrak-APC fate mapping and niche assessment were performed on Dox-suppressed offspring at postnatal day (P)-10, 30, 60, and 120.

(B) Representative images of tdTomato and perilipin (Plin1) immunostaining of iWAT and gWAT sections examining APC-adipocyte fate mapping from mice described in (A).

(C) Representative images of SVPs from iWAT depots examining AdipoTrak-APC occupancy and density from mice described in (A).

Scale bars = 100 μm. See also Figure S1.

To investigate other Pdgfrβ loss of function-induced changes in WAT remodeling, we performed histological staining, immunohistochemistry, and qPCR analysis on control and mutant WATs. Strikingly, Masson's trichrome collagen staining revealed fibrotic tissue replacement throughout Pdgfrβ^{AT}KO subcutaneous and visceral WAT sections (Figures 2F and S2I). In conjunction with these findings, Pdgfrβ^{AT}KO iWAT and gWAT depots had increased expression of fibroblast markers (e.g., Col1a1) (Figures S2J and S2K).[23] A common feature of dysfunctional WAT is inflammation.[24] Indeed, F4/80, an inflammatory marker,[25] staining exposed more immune cell infiltration into the Pdgfrβ^{AT}KO WAT depots, suggesting adipocyte and tissue cell death (Figures 2G and S2L). Moreover, inflammatory markers (e.g., TNFa) were upregulated in mutant WAT compared to controls (Figures S2M and S2N). Lipodystrophy is often associated with elevated serum triglycerides and ectopic lipid storage.[26] Indeed, serum triglycerides were slightly elevated in mutant mice, and we also observed variegated liver lipid storage at P60 (Figures S2O and S2P). Overall, deleting Pdgfrβ within the adipose lineage increases the demand for lipid storage and facilitates adipose dysfunction in adult WAT.

Adipose lineage platelet-derived growth factor receptor beta function is critical for diet-induced obesity and white adipose tissue expansion

To probe if Pdgfrβ deficient adipose lineage cells could be triggered to differentiate, we fed P60 Control^{AT} and Pdgfrβ^{AT}KO male mice a high-fat diet (HFD; 60% fat) for 12 weeks (Figure 3A). NMR body composition analysis revealed that feeding Pdgfrβ^{AT}KO mice an HFD increased

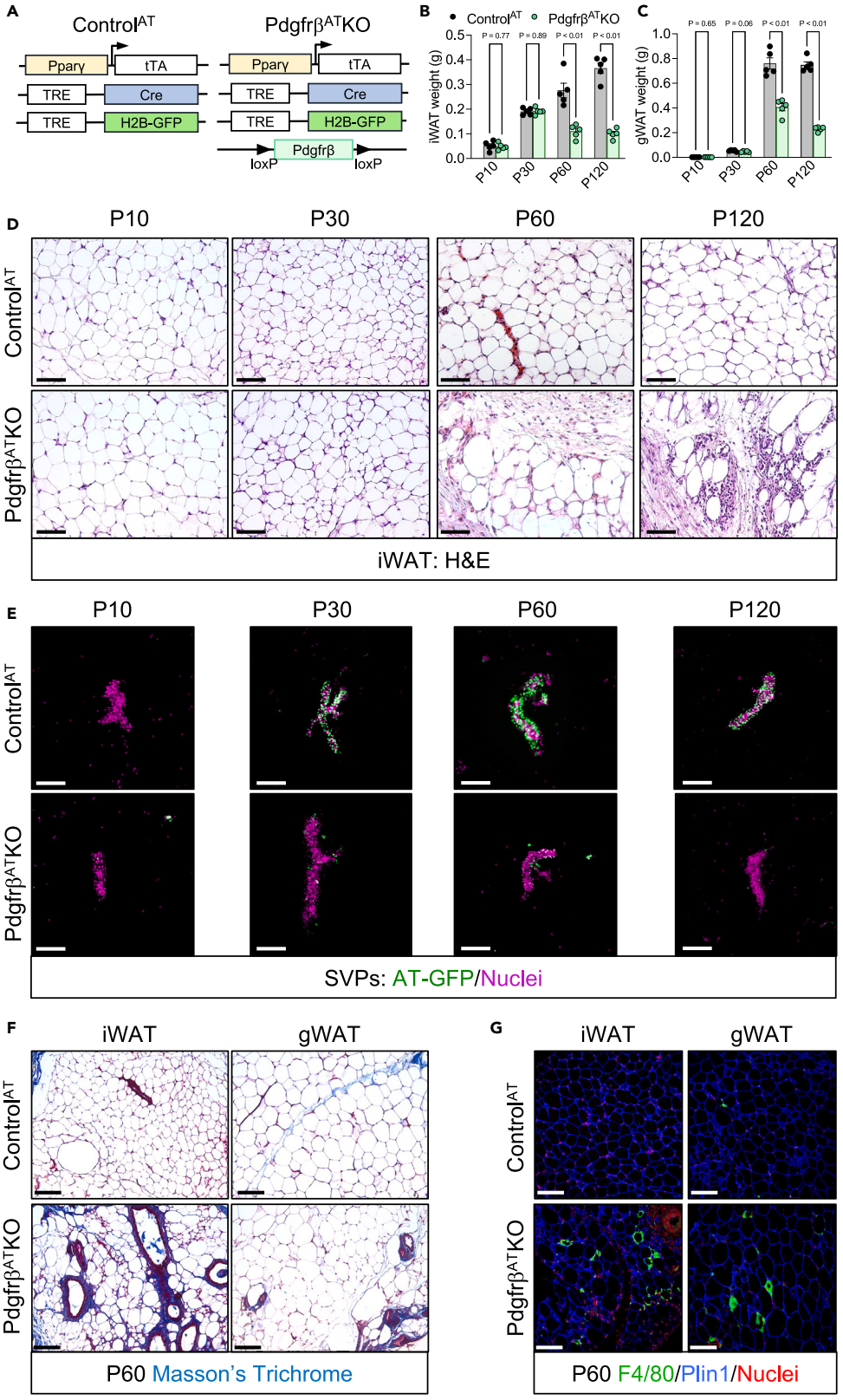
A
Control^AT
Pdgfrβ^ATKO
Pparγ
tTA
TRE
Cre
H2B-GFP
Pdgfrβ
loxP
B
Control^AT
Pdgfrβ^ATKO
iWAT weight (g)
P = 0.77
P = 0.89
P < 0.01
P < 0.01
P10
P30
P60
P120
C
gWAT weight (g)
P = 0.65
P = 0.06
P < 0.01
P < 0.01
D
iWAT: H&E
E
SVPs: AT-GFP/Nuclei
F
iWAT
gWAT
P60 Masson's Trichrome
G
P60 F4/80/Plin1/Nuclei

Figure 2. Pdgfrβ regulates WAT homeostasis and function

(A) Diagram of the allelic combination used to generate Control^{AT} and Pdgfrβ^{AT}KO mice.

(B and C) iWAT (inguinal WAT) (B) and gWAT (perigonadal WAT) (C) from non-Dox suppressed Control^{AT} and Pdgfrβ^{AT}KO male mice at P-10, 30, 60, and 120 (n = 5 mice/group).

(D) Representative images of hematoxylin and eosin (H&E) staining of WAT sections from mice described in (B).

(E) Representative images of SVPs from iWAT depots from mice described in (B).

(F) Representative images of Masson trichrome collagen staining from iWAT and gWAT depots from Control^{AT} and Pdgfrβ^{AT}KO male mice at P60.

(G) Representative images of F4/80 immunostaining of iWAT and gWAT sections from Control^{AT} and Pdgfrβ^{AT}KO male mice at P60.

Scale bars = 100 μm. Data are represented as mean with individual data points ±SEM. Students unpaired t-test was used to analyze significance. See also Figure S2.

body fat composition. However, mutant mice retained a 50% decrease in overall body fat composition compared to control mice (Figure 3B). While control and mutant mice demonstrated comparable glucose intolerance and serum insulin levels, Pdgfrβ^{AT}KO mice maintained elevated serum triglyceride levels (Figures 3C–3E). Additionally, WAT weights remained significantly lower in mutants than controls (Figure 3F). Interestingly, mutant liver weights were nearly double the controls, whereas other organ weights appeared similar, except spleen, which weighed slightly more in mutant mice (Figure 3G).

While Pdgfrβ^{AT}KO depots expanded under HFD administration, they did not appear to have normal texture, appearing rubbery. To understand how mutant WAT depots expanded under HFD conditions, we performed H&E and Masson Trichrome staining. Like NCD conditions, we found continued disruption of iWAT and gWAT adipocyte size and lower gene expression of adipocyte markers in iWAT, not gWAT, depots (Figures S3A–S3C). Additionally, we found an increase in fibrotic staining within mutant WAT sections compared to control depots (Figures 3H and S3D). Fibrotic tissue appearance was also associated with increased fibrotic genetic markers such as Col1a1 (Figures S3E and S3F). Consistent with HFD-induced WAT dysfunction, mutant WAT depots had an increase in F4/80-positive macrophage infiltration compared to control WATs (Figures 3I and S3G). In agreement, mutant WAT depots showed elevated levels of pro-inflammatory genes compared to control tissues (Figures S3H and S3I). Next, we evaluated if HFD could alter AdipoTrak-labeled APC-niche residence. Analysis of SVPs revealed that controls remained in niche positions, whereas mutants did not—resembling NCD conditions (Figures S3J and S3K).

Because Pdgfrβ^{AT}KO mutant WAT depots were heavier, but adipocyte size remained comparable to NCD after HFD treatment, we measured triglyceride levels between NCD and HFD control and mutant mice. As anticipated, HFD increased WAT triglyceride levels in control depots compared to NCD quantities (Figure 3J). In opposition, Pdgfrβ^{AT}KO HFD-fed mice contained less WAT triglycerides than controls and remained comparable to mutant NCD conditions, suggesting limited triglyceride accumulation within mutant WAT (Figure 3J). Coinciding with reduced WAT triglyceride accumulation, Pdgfrβ^{AT}KO livers had an abundance of ectopic lipid droplets after HFD feeding (Figure 3K). The histopathological features of liver steatosis led us to evaluate if Pdgfrβ^{AT}KO adipose lineage cells remained defective in adipogenesis after HFD. While we observed several lipid-positive cells throughout the Pdgfrβ^{AT}KO cultures under the HFD state, differentiation was significantly less than in HFD-control cultures (Figure S3L). Consistent with reduced lipid presence, mature adipocyte markers were considerably lower in mutant cultures compared to controls (Figure S3M). Together, these data suggest that changes in fat content upon HFD in Pdgfrβ^{AT}KO mice likely emanated from compensatory mechanisms, such as ectopic liver lipid storage, and that Pdgfrβ^{AT}KO APCs remain adipogenically impaired.

Progenitor platelet-derived growth factor receptor beta deletion appears to induce a fate change

To investigate if Pdgfrβ directly regulated APC dynamics, we evaluated the AdipoTrak-driven TRE-H2B-GFP (H2B, Histone 2B) reporter activity. Notably, the tTA-driven H2B-GFP can be stably incorporated into the chromatin of proliferating adipose lineage cells. Additionally, lineage-positive cells will be continually green if they continue to express Pparγ. However, changes in GFP expression can be observed if the number of progenitors is reduced or if Pparγ expression is stopped, which could be secondary to cellular fate changes.[27] To provide a broad overview of the tissue GFP expression, we evaluated whole-mount fluorescence imaging of iWAT and gWAT. The imaging revealed that iWAT GFP intensity appeared reduced, potentially suggesting changes in APC lineage availability (Figure 4A). Yet, gWAT depot GFP intensity appeared similar which could be attributed to tissue thickness or the compact size of the Pdgfrβ^{AT}KO gWAT depots compared to the larger control depot (Figure 4A). To analytically assess if ablating Pdgfrβ-induced changes in AdipoTrak-APC progenitor, we used flow cytometric analysis to evaluate APC-GFP+ number between control and mutant mice (Figures 4B and S4A). As hinted from the whole mount imaging, Pdgfrβ^{AT}KO iWAT depots had significantly lower GFP-positive cell number (~10% reduction). On the other hand, Pdgfrβ^{AT}KO gWAT had reduced GFP cell number (~5%) compared to controls, but not as affected as iWAT (Figures 4C and S4B). These data suggest Pdgfrβ^{AT}KO depots have fewer committed Pparγ-marked APCs.

Changes in GFP number lead us to probe the possibility that Pdgfrβ deletion might change APC fate. To test this, we combined the Rosa26-flox-stop-flox-tdTomato allele into Pdgfrβ^{AT}KO mice, permanently marking adipose progenitor cells and all descendants (Figure 4D).[28] We found an increase in tdTomato-positive cells within the Pdgfrβ^{AT}KO WAT depots compared to the control (Figures 4E and S4C). This data suggested that these tdTomato-positive cells derived from a Pparγ lineage—and contained the Pdgfrβ deletion but were no longer in the active (less GFP) adipose lineage. Yet, what could these Pparγ-derived Pdgfrβ-deficient tdTomato-positive cells be? The prominent effect on immunological cell changes led us to hypothesize that Pdgfrβ-deficient APCs might exist as an alternative cell type, such as macrophages. Toward this end, we stained WAT sections from control and Pdgfrβ^{AT}KO mice for tdTomato and Mac2, a general macrophage cell marker.[29] As expected, in both models, the AdipoTrak-driven tdTomato reporter colocalized with perilipin positive

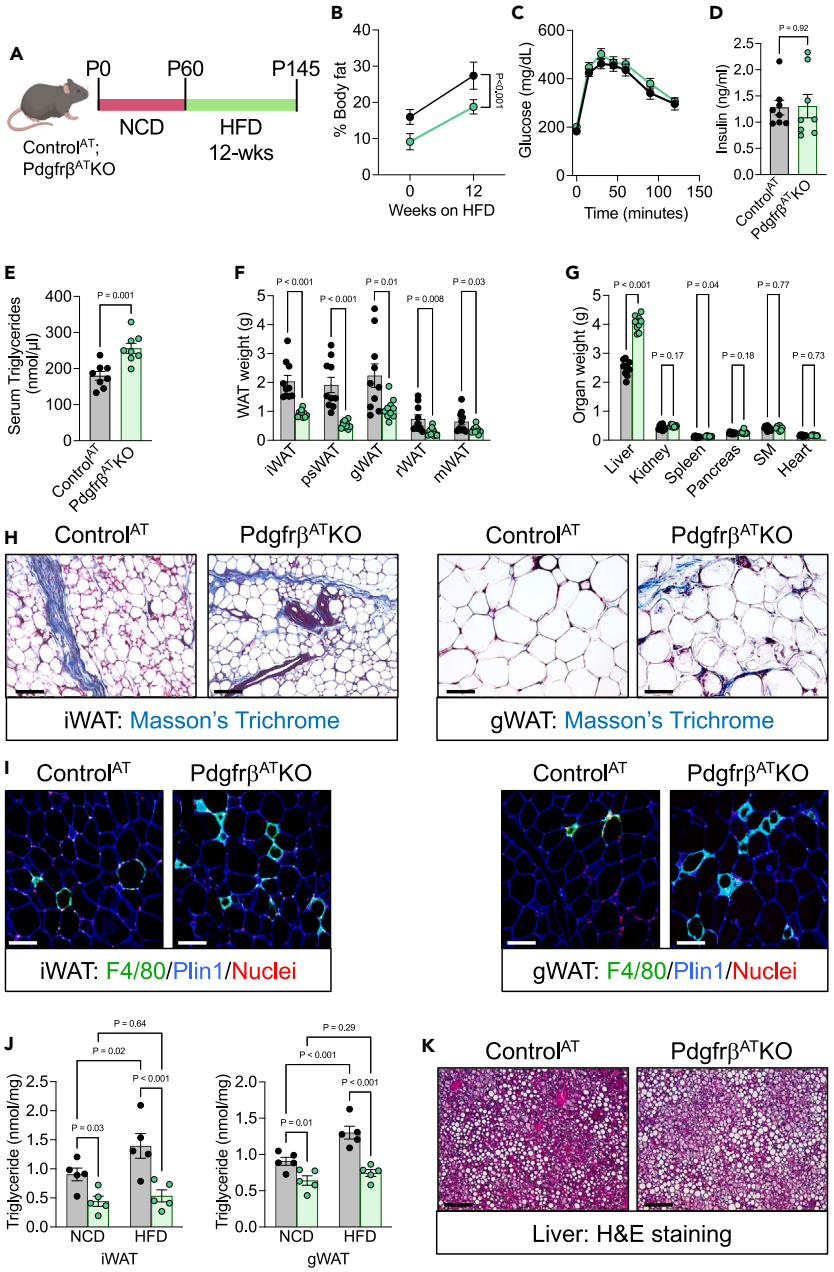

Figure 3. Pdgfrβ deletion averts high fat diet induced WAT expansion

(A) Experimental design: Starting at P60, Control^{AT} and Pdgfrβ^{AT}KO male mice were fed an HFD (60% fat) for 12 weeks.

(B) NMR body fat composition analysis before and after HFD administration (n = 14 mice/group).

(C) Glucose tolerance test performed on mice described in (A) after 12 weeks HFD administration (n = 14 mice/group).

(D) Fasted serum insulin levels from mice described in (A) (n = 8 mice/group).

(E) Serum triglyceride levels from mice described in (A) (n = 8 mice/group).

(F) WAT weights from mice described in (A) (n = 10 mice/group) (inguinal (iWAT), periscapular (psWAT), perigonadal (gWAT), retroperitoneal (rWAT), and mesenteric (mWAT)).

(G) Organ weights from mice described in (A) (n = 10 mice/group) (SM = skeletal muscle).

(H) Representative images of Masson's trichrome collagen staining of iWAT (left) and gWAT (right) from mice described in (A).

(I) Representative images of F4/80 immunostaining of iWAT (left) and gWAT (right) sections from mice described in (A).

(J) Triglyceride levels from iWAT and gWAT depots from Control^{AT} and Pdgfrβ^{AT}KO male mice fed NCD or HFD (n = 5 mice/group).

(K) Representative images of hematoxylin and eosin (H&E) staining of liver sections from mice described in (A).

Scale bars = 100 μm. Data are represented as mean with individual data points ±SEM. Students unpaired t-test or two-way ANOVA test were used to analyze significance. See also Figure S3.

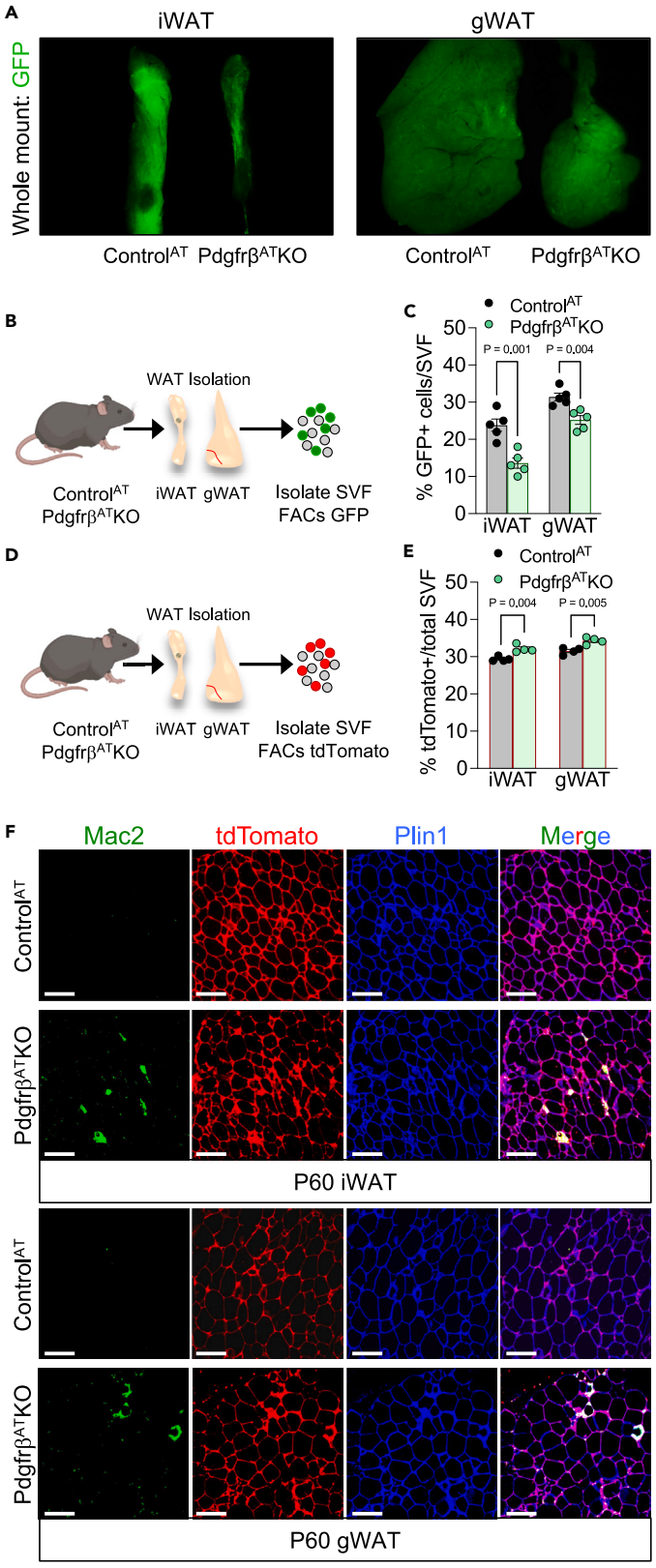
A
iWAT
gWAT
Whole mount: GFP
Control^AT
PdgfrβATKO
Control^AT
PdgfrβATKO
B
WAT Isolation
Control^AT
PdgfrβATKO
iWAT gWAT
Isolate SVF
FACs GFP
C
Control^AT
PdgfrβATKO
% GFP+ cells/SVF
P = 0.001
P = 0.004
iWAT gWAT
D
WAT Isolation
Control^AT
PdgfrβATKO
iWAT gWAT
Isolate SVF
FACs tdTomato
E
Control^AT
PdgfrβATKO
% tdTomato+/total SVF
P = 0.004
P = 0.005
iWAT gWAT
F
Mac2
tdTomato
Plin1
Merge
Control^AT
PdgfrβATKO
P60 iWAT
Control^AT
PdgfrβATKO
P60 gWAT

Figure 4. Pdgfrβ regulates APC fate

(A) Representative images of whole-mount fluorescence of AdipoTrak-GFP from iWAT (left) and gWAT (right) depots from Control^{AT} and Pdgfrβ^{AT}KO mice fed NCD.

(B and C) Experimental design (B): At P60, SV cells were isolated from iWAT and gWAT depots from Control^{AT} and Pdgfrβ^{AT}KO. AdipoTrak-GFP APC number was determined by flow cytometry (C) (n = 5 mice/group).

(D and E) Experimental design (D): At P60, the SVF was isolated from iWAT and gWAT depots from Control^{AT} and Pdgfrβ^{AT}KO. AdipoTrak-tdTomato APC number was determined by flow cytometry (E) (n = 4 mice/group).

(F) Representative images of Mac2 and tdTomato immunostaining of iWAT and gWAT depots from Control^{AT} and Pdgfrβ^{AT}KO male mice at P60.

Scale bars = 100 μm. Data are represented as mean with individual data points ±SEM. Students unpaired t-test was used to analyze significance. See also Figure S4.

adipocytes. However, in control iWAT and gWAT sections, we did not observe colocalization between tdTomato and Mac2 staining (Figure 4F). In stark contrast, we observed large overlap between Pdgfrβ^{AT}KO-tdTomato positive cells and Mac2 staining, suggesting a possible fate change. Notably, the cells in the fibrotic tissue area did not express tdTomato (Figure S4D). Moreover, flow cytometric analysis revealed an increase in overall macrophage abundance within mutant WAT depots compared to control tissues (Figure S4E). Extending these findings, we FACs evaluated CD68 and tdTomato overlap in control and mutant WAT depots. In control samples, we observed limited correspondence between reporter and CD68 whereas, Pdgfrβ^{AT}KO-tdTomato cells were predominantly CD68 positive (Figure S4F). Overall, although Pdgfrβ deletion causes less adiposity, the underlying genetic basis of this phenotype is suggestive of an altered adipose-to-macrophage lineage switch.

Adult platelet-derived growth factor receptor beta signaling is required for niche localization but not adipose lineage identity

To probe if Pdgfrβ induces potential lineage changes during the adult homeostatic phase, we doxycycline suppressed control and Pdgfrβ^{AT}KO mice from conception until P60 (Figures S4G and S4H). At P60, we removed Dox to delete Pdgfrβ within AdipoTrak-positive cells, allowing us to assess if Pdgfrβ induces adult lineage transitions (Figure S4I). Throughout the six-weeks, Pdgfrβ^{AT}KO mice stagnated in WAT expansion, as we previously observed[19] (Figure S4J). Next, we isolated SV cells from iWAT and gWAT depots from control and mutant mice to evaluate AdipoTrak-GFP positive cell number. Flow cytometric analysis showed comparable GFP reactivation after Dox suppression, suggesting that Pparγ was active and the AdipoTrak APC lineage seemed intact (Figure S4K). Next, we assessed, using immunostaining, the presence of Mac2-postive macrophages between E0 Dox-suppressed control and Pdgfrβ^{AT}KO; however, we found no differences (Figure S4L). In support of this notion, directed qPCR analysis revealed similar levels of pro- and anti-inflammatory markers (Figure S4M). Pdgfrβ can regulate niche interaction to control adipose tissue growth; therefore, we evaluated SVPs from control and mutant iWAT depots. As previously reported, SVPs isolated from Pdgfrβ^{AT}KO had fewer GFP+ cells per SVP than controls, suggesting that Pdgfrβ regulates niche regulation but not lineage identity in adult WATs[19] (Figures S4N and S4O).

Embryonic expression of platelet-derived growth factor receptor beta is required for adult adipose tissue homeostasis

The data suggest that deleting Pdgfrβ in adult WAT induces APC-niche mis-localization to slow WAT growth. Yet, constitutively deleting Pdgfrβ diminished the active AdipoTrak+ APC lineage, suggesting a possible developmental lineage fate switch. To investigate if Pdgfrβ deletion—developmentally—alters adult adipose lineage commitment and trajectory, we employed embryonic lineage tracing strategies coupled with Pdgfrβ deletion to monitor only adult APC fate and function.[14] To do so, we doxycycline suppressed Pdgfrβ^{AT}KO from E10.5 onwards (only deleting Pdgfrβ in the adult progenitor pool) and monitored completed WAT development at P45 or analyzed adult adipose tissue homeostasis at four months (P120) of age (Figures 5A and S5A). At P45, the E10.5 Dox-suppressed Pdgfrβ^{AT}KO mice mirrored Control^{AT} mice; that is, they had similar body weight, food intake, fat content, and WAT histology (Figures 5B, 5C, and S5B–S5D). Molecular analysis indicated that the P45 depots were relatively unaffected, with typical adipocyte size and normal levels of mature adipocyte and inflammatory markers (Figures S5E–S5G). However, *in vitro* adipogenic assessment revealed suppressed adipogenesis, suggesting normal tissue development but potential adult progenitor defects (Figures S5H and S5I).

We continued to assess the E10.5 Pdgfrβ^{AT}KO cohort over the ensuing months and observed a decrease in fat content, whereas controls continued to increase fat mass (Figures 5C and S5J). Even though E10.5 Pdgfrβ^{AT}KO mice had less adipose tissue, glucose tolerance remained similar between control and mutants (Figure 5D). By four months of age, the E10.5 Pdgfrβ^{AT}KO mice had approximately half the body fat and smaller adipose depots, but similar food intake compared to four-month-old controls (Figures 5E, 5F, and S5K). Histological studies indicated that the mutants had enlarged adipocytes and disrupted WAT architecture (Figures 5G and S5L). Gene expression analyses of adipose depots revealed reduced levels of mature adipocyte markers, including Pparγ (Figure S5M). Interestingly, unlike the constitutive Pdgfrβ deletion model, fibrotic tissue presence appeared comparable between control and mutant WAT (Figures 5G and S5N). In contrast, histological imaging revealed many crown-like structures surrounding adipocytes within Pdgfrβ^{AT}KO iWAT and gWAT sections (Figure 5G). In support of this notion, Mac2 immunostaining showed an abundance of macrophages within Pdgfrβ^{AT}KO WAT sections (Figures 5H and 5I). Additionally, pro-inflammatory markers were also upregulated in Pdgfrβ^{AT}KO iWAT and gWAT depots, supporting immunological changes within mutant WATs (Figures 5J and S5O). Overall, deleting Pdgfrβ within the E10.5-specified adult APC lineage results in dysfunctional WAT growth and inflammation.

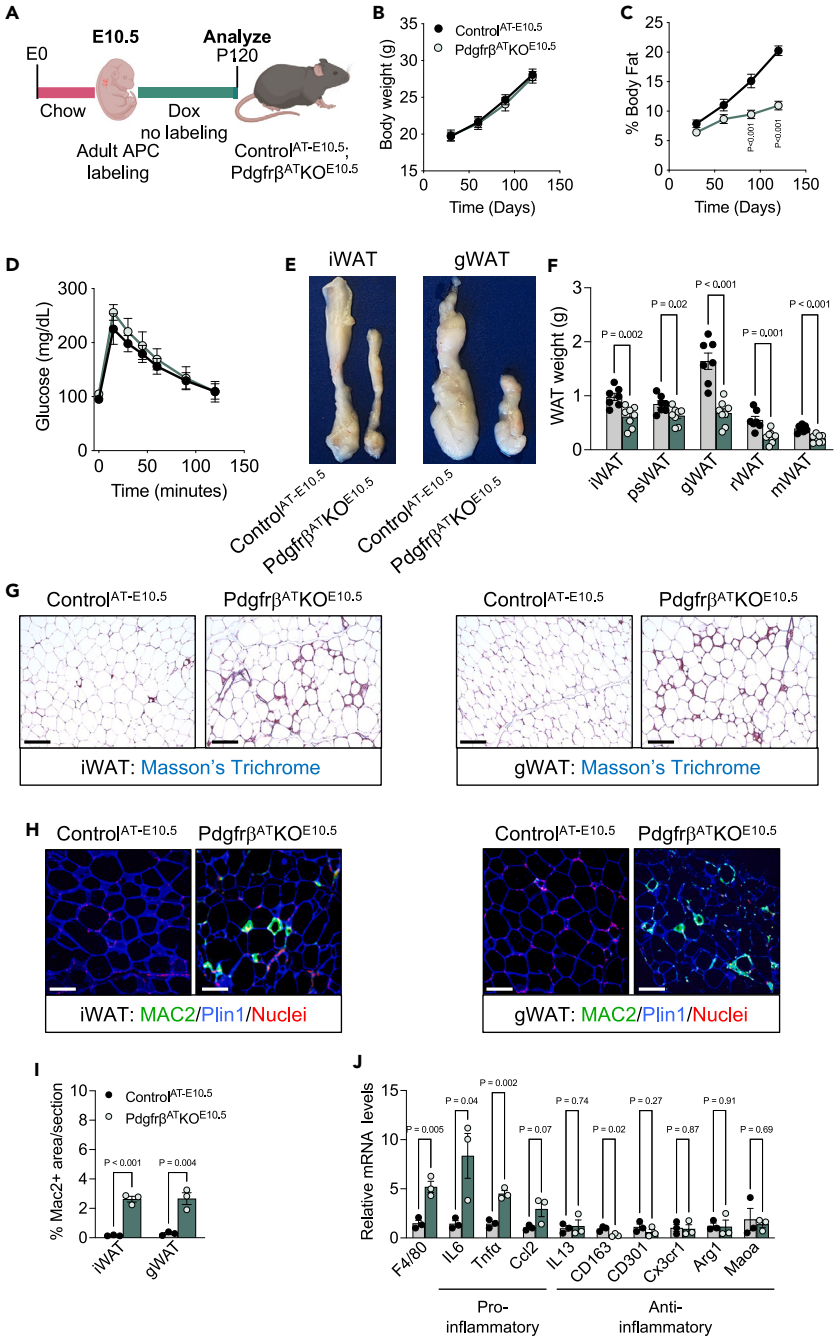

Figure 5. Embryonic Pdgfrβ deletion regulates adult APC function

(A) Experimental design: Control^{AT} and Pdgfrβ^{AT}KO mice were time mated. At E10.5 pregnant females were administered Dox diet (preventing further Pdgfrβ deletion). Offspring were maintained on Dox diet and evaluated at P120.

(B) Body weight curve from mice described in (A) at P30, P60, P90 and P120 (n = 7–8 mice/group).

(C) Serial NMR body composition analysis were performed on offspring described in (A) at P30, P60, P90 and P120 (n = 7–8 mice/group).

(D) Glucose tolerance test was performed on offspring described in (A) at P120 (n = 7–8 mice/group).

(E) Representative photograph of iWAT and gWAT depots from mice described in (A).

(F) WAT weights from offspring described in (A) (n = 7–8 mice/group).

(G) Representative images of Masson's trichrome staining of iWAT (left) and gWAT (right) sections from mice described in (A).

(H) Representative images of Mac2 immunostaining of iWAT (left) and gWAT (right) sections from mice described in (A).

Figure 5. *Continued*

(I) Quantification of Mac2 immunostaining from images described in (H) (n = 3 mice/group).

(J) Relative mRNA levels of denoted pro- and anti-inflammatory genes within iWAT depots from mice described in (A) (n = 3 mice/group).

Scale bars = 100 μm. Data are represented as mean with individual data points ±SEM. Students unpaired t-test was used to analyze significance. See also Figure S5.

Embryonic expression of platelet-derived growth factor receptor beta regulates adipose lineage specification

Because E10.5 Pdgfrβ deletion impairs adipose tissue homeostatic growth, we asked if E10.5 Dox Pdgfrβ^{AT}KO cells arrived in the correct anatomical anlagen.[1] Toward this end, we lineage traced Dox suppressed control or Pdgfrβ^{AT}KO E10.5 cells by tdTomato indelible labeling and monitored their recruitment to WAT depots at P120 (Figure 6A). In control WAT sections, we observed peri-vascular tdTomato-labeling and numerous adipocytes were tdTomato positive (Figures 6B and 6C). In contrast, Pdgfrβ^{AT}KO tdTomato-positive cells appeared mis-localized to the vasculature and did not lineage trace into mature adipocytes (Figures 6B and 6C). Interestingly, E10.5 Pdgfrβ^{AT}KO tdTomato-positive cells resided interstitially, in-between, or surrounding adipocytes, and appeared in dense nuclear clusters (Figure 6B). To test if Pdgfrβ-deficient cells were adipogenic, we isolated SV cells from iWAT depots from control and mutant mice. Both lipid droplet imaging and adipocyte gene expression indicated reduced adipocyte differentiation (Figures 6D and 6E).

Because Pdgfrβ-deficient cells appeared interstitially in dense clusters, we hypothesized these cells might be macrophages.[30] To test this notion, we performed Mac2 (macrophage) immunostaining on control and mutant WAT sections. In control sections, we observed many tdTomato cells, but Mac2 staining was limited and did not colocalize with tdTomato. In contrast, we found significant correspondence between tdTomato-positive cells and Mac staining within Pdgfrβ^{AT}KO WAT sections (Figures 6G and S6A). To continue to evaluate E10.5 Pdgfrβ-deficient cell identity, we performed flow cytometric analysis on macrophage cell surface marking. While several studies have suggested correspondence in adipocyte and macrophage lineages,[31] we observed a slight overlap (~5–8%) in control E10.5 AdipoTrak-tdTomato cells and CD68. Even when forced with HFD—causing macrophage activation and accrual—E10.5 cells remained restricted to the adipose lineage (Figures S6B and S6C).[30] Conversely, within NCD Pdgfrβ^{AT}KO iWAT and gWAT depots, CD68 cells were tdTomato-positive, suggesting they emanated from a Pparγ expressing cell (Figure 6F). Together, these data suggest that E10.5 Pparγ+ cells lacking Pdgfrβ favor macrophage lineage specification rather than adipose lineage development.

Platelet-derived growth factor receptor beta -deficient cells represent macrophages upon white adipose tissue arrival

Unexpectedly, WAT dysfunction was inconspicuous at P45 when E10.5 Pdgfrβ ablated APCs should be infiltrating the depots (Figure 1). Additionally, gene expression profiling of WAT depots from Dox-suppressed E10.5 control and mutant mice revealed comparable levels of pro-inflammatory and anti-inflammatory markers known to be induced by WAT disruption (Figure 5J).[32] Nevertheless, by P120, Pdgfrβ-deficient WATs became non-adipogenic and inflamed (Figure 5). Given these changes in mutant WAT function between P45 and P120, we assessed the number of tdTomato marked and CD68-positive cells between the E10.5 Dox-suppressed control and mutant WAT depots. While control tdTomato cell number remained constant between P45 and P120, Pdgfrβ-deficient cells increased, suggesting these cells accrued or expanded as WAT became impaired (Figure S6D). Notably, at P45, we observed that Pdgfrβ-deficient WAT depots displayed more tdTomato-marked cells than control depots. Similarly, CD68 numbers remained relatively constant between P45 and P120 in control depots, whereas Pdgfrβ-deficient WAT exhibited an increase in CD68 cell numbers (Figure S6E). Particularly, irrespective of time, CD68-positive cells were predominantly marked by tdTomato in mutant WAT compared to control, suggesting that E10.5 Pdgfrβ-deficient cells are macrophages upon tissue entry (Figures S6F and S6G). In agreement, Mac2 immunostaining confirmed the presence of macrophages at P45, which overlapped with tdTomato within E10.5 Pdgfrβ-deficient WAT sections (Figures S6H and S6I). Furthermore, unlike control sections, we did not observe fate mapping of tdTomato APCs into adipocytes in E10.5 Pdgfrβ-deficient WAT sections at P45. These findings suggest that Pdgfrβ ablation in E10.5 APCs results in an adipose-to-macrophage lineage conversion, resulting in less adipogenesis to elicit WAT dysfunction and macrophage accrual.

Platelet-derived growth factor receptor beta activation maintains adipose lineage expansion

Given the impact of Pdgfrβ ablation on adipose lineage decisions, we evaluated the potential of Pdgfrβ signaling to regulate adult adipogenesis and adipose lineage dynamics. As previously reported,[33] continual activation of Pdgfrβ signaling by the administration of recombinant murine Pdgf-BB ligand limited the appearance of lipid-positive adipocytes and suppressed mature adipocyte gene expression (Figures 7A, 7B and S7A). Centering on Pdgfrβ induced APC regulation, we queried the status of APC marker gene expression after Pdgf-BB administration (Figure 7C). Irrespective of vehicle or Pdgf-BB treatment "preadipocyte" markers such as Pparγ, Zfp423, and Pref-1, remained equivalent (Figure 7D).[17,21,34] The lack of effect of Pdgfrβ activation on adult APC stemness genes, led us to test if Pdgfrβ signaling increased APC proliferative potential. To do so, we treated P45 Dox suppressed E10.5 control mice with vehicle or recombinant Pdgf-BB protein along with Bromodeoxyuridine (BrdU), a DNA nucleotide analog to monitor proliferation, for five consecutive days (Figure 7E).[35] Flow cytometric analysis revealed BrdU incorporation into control tdTomato cells (Figures 7F and 7G). Strikingly, Pdgf-BB increased BrdU incorporation and amplified the total cellular population of E10.5 tdTomato cells (Figures 7F–7H). These data suggest that Pdgfrβ activation stimulates APC self-renewal *in lieu* of stemness.

To uncover how Pdgfrβ signaling promotes APC proliferation, we evaluated downstream effectors of Pdgfrβ signaling (Figure 7I). Recent reports have suggested that Pdgfrβ signaling via Stat1 phosphorylation mediates several responses involved in thermogenesis,

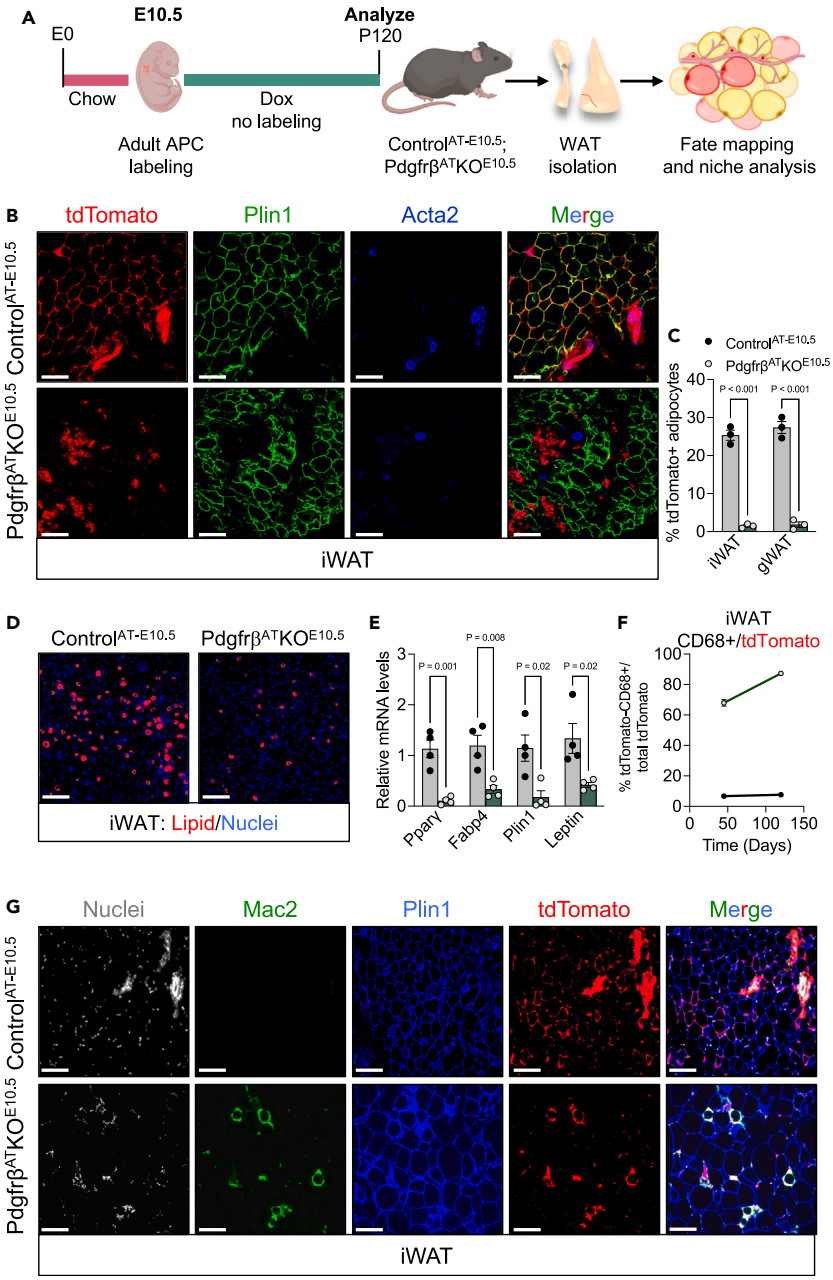

Figure 6. Adult Pdgfrβ deficient APCs are non-adipogenic and resemble macrophages

(A) Experimental design: Control^{AT} and Pdgfrβ^{AT}KO mice were time mated. At E10.5 pregnant dams were administered Dox diet. Offspring were maintained on Dox diet and evaluated at P120.

(B) Representative images of tdTomato, Plin1, and Acta2 immunostaining of iWAT sections from mice described in (A).

(C) Quantification of tdTomato adipocyte fate mapping in iWAT and gWAT sections from mice described in (A) (n = 3 mice/group).

(D) Representative images of *in vitro* adipogenesis of SVF cultures isolated from iWAT depots from mice described in (A). Cultures were stained with LipidTox to examine lipid presence.

(E) Relative mRNA levels of adipocyte markers from *in vitro* adipogenic cultures described in (D) (n = 4 mice/group).

(F) Flow cytometric analysis of the percent overlap of CD68 and AdipoTrak-tdTomato over total tdTomato cells present in the SVF of iWAT depots from mice described in (A) (n = 3 mice/group). G) Representative images of Mac2, tdTomato, and Plin1 immunostaining of iWAT sections from mice described in (A). Scale bars = 100 μm. Data are represented as mean with individual data points ±SEM. Students unpaired t-test was used to analyze significance. See also Figure S6.

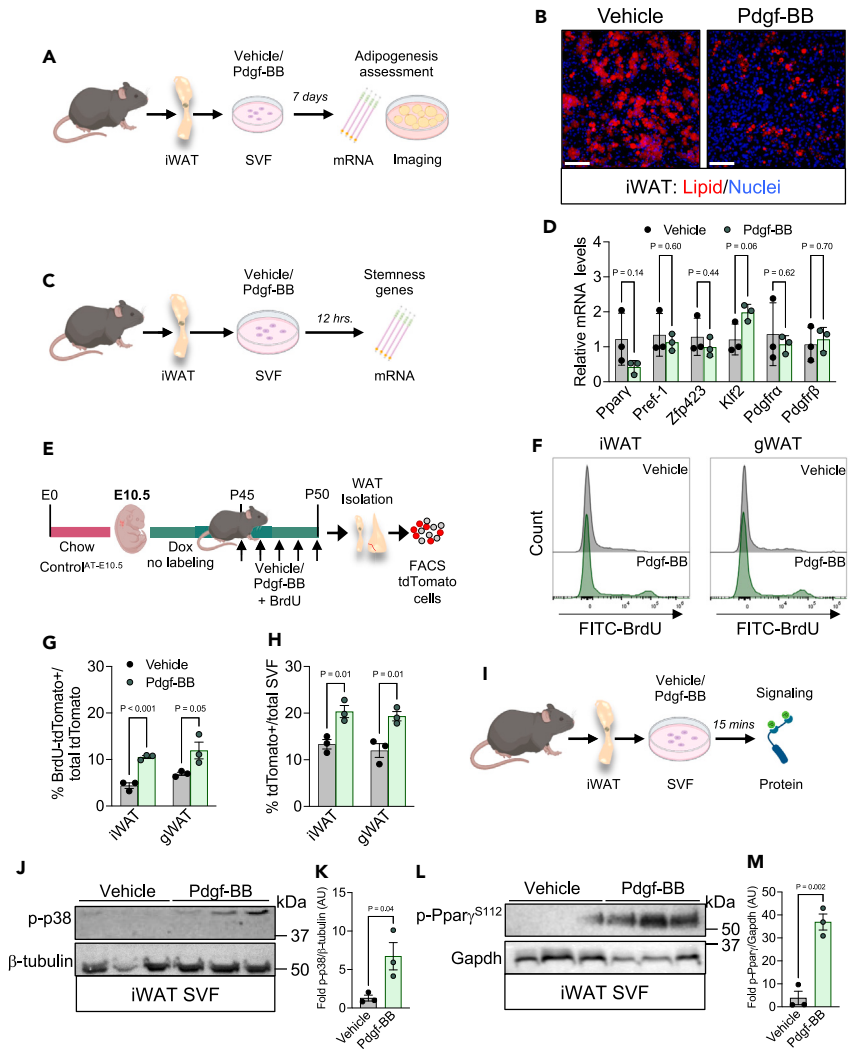

Figure 7. Pdgfrβ signaling via p38/MAPK maintains a pool of proliferative APCs

(A) Experimental design: The SVF was isolated from iWAT depots from Control^{AT} mice at P45. Cells were induced with adipogenic media in the presence of vehicle or Pdgf-BB (25 ng/mL) for seven days. Cultures were imaged and assessed for adipocyte marker gene expression.

(B) Representative images of *in vitro* adipogenesis from cultures described in (A).

(C and D) Experimental design (C): The SVF was isolated from iWAT depots from Control^{AT} mice at P45. Cells were cultured in the presence of vehicle or Pdgf-BB (25 ng/mL) for 12 h. APC stemness genes were assessed (D) (n = 3 mice/group).

(E) Control^{AT} mice were time mated and at E10.5 pregnant dams were administered Dox diet. Offspring were maintained on Dox diet and at P45 were administered one dose of vehicle or Pdgf-BB along with BrdU for five consecutive days.

(F) Representative BrdU histograms from iWAT and gWAT depots from mice described in (E).

(G) BrdU incorporation into APCs (tdTomato) from iWAT and gWAT depots from mice described in (E) (n = 3 mice/group).

(H) tdTomato number from iWAT and gWAT depots from mice described in (E) (n = 3 mice/group).

(I–M) Experimental design (I): The SVF was isolated from iWAT depots from Control^{AT} mice at P45. Cells were cultured in the presence of vehicle or Pdgf-BB (25 ng/mL) for 15 min. Lysates were immunoblotted and quantified against p38/MAPK (J,K) and Pparγ (L and M) phosphorylation (n = 3 mice/group).

Scale bars = 100 μm. Data are represented as mean with individual data points ±SEM. Students unpaired t-test was used to analyze significance. See also Figure S7.

atherosclerosis and Koski overgrowth syndrome.[36–38] However, Stat1 phosphorylation remained comparable between control and mutant tdTomato E10.5 cells after Pdgf-BB treatment (Figure S7B). Instead, by flow cytometry, we observed an increase in p38/Mapk phosphorylation in response to Pdgf-BB treatment (Figure S7C).[39] These observations were supported by Western blot analysis of p38/MAPK phosphorylation after Pdgf-BB stimulation *in vitro* (Figures 7J and 7K). Additionally, Western blot analysis confirmed that Pdgfrβ could be phosphorylated by Pdgf-BB ligand administration (Figure S7D and S7E). To examine the requirement of Pdgfrβ in p38/MAPK signaling, we treated SV cells isolated from Pdgfrβ^{AT}KO mice with Pdgf-BB. We found that p38/MAPK could not be phosphorylated in Pdgfrβ-deficient cells in response to

Pdgf-BB, suggesting that this ligand-receptor combination initiates p38/MAPK phosphorylation (Figure S7F and S7G). Activation of p38/MAPK pathways is known to phosphorylate Pparγ, specifically at serine 112, to block adipogenic progression.[40,41] We tested if Pdgfrβ-p38/MAPK signaling could phosphorylate Pparγ and found that Pdgf-BB treatment increased Pparγ phosphorylation at serine 112, suggesting a potential anti-adipogenic mechanism (Figures 7L and 7M). To test the Pdgfrβ-induced p38/MAPK activation requirement on Pparγ phosphorylation, we chemically inhibited (SB202190) p38/MAPK phosphorylation in the presence of Pdgf-BB administration.[42] The SB202190 and Pdgf-BB treatment combination reduced Pparγ phosphorylation at serine 112, suggesting the requirement of p38/MAPK in mediated Pdgrfβ signaling (Figures S7H and S7I). Overall, Pdgfrβ signaling maintains the APC proliferative pool by p38/MAPK and Pparγ phosphorylation.

DISCUSSION

The data here highlight an essential role for the embryonic specification of adult adipocyte progenitors in regulating mature adipose tissue expansion and function. In agreement, our studies identify Pdgfrβ as an embryonic molecular determinant of the adult APC lineage. Strikingly, deleting Pdgfrβ within the adipose lineage results in a paucity of adipose tissue with immune cell infiltration, which cannot be recovered by HFD administration. Of note, control and mutant mice have comparable glucose clearance responses, which may indicate compensatory mechanisms (i.e., muscle) and shifts in energy balance. Lineage tracing studies reveal that Pdgfrβ-deficient adult APCs (E10.5 deletion and marking) undergo lineage conversion to macrophages. These macrophages expand and become pro-inflammatory in response to HFD administration. Mechanistically, our data appear to suggest that Pdgfrβ serves as a linchpin in APC lineage expansion via p38/MAPK. Moreover, Pdgfrβ signaling upholds the APC state by preventing adipogenesis through Pparγ^{Ser112} phosphorylation. Thus, we propose a model in which Pdgfrβ is a critical regulator of embryonic adipose-to-macrophage lineage determination and confinement. Genetic lineage tracing and molecular analysis support this hypothesis and suggest that Pdgfrβ preserves and expands the APC lineage to impact WAT growth and function.

Pdgfrβ marks the adipose lineage and appears to regulate tissue-resident APCs.[15,34,43] In addition to APCs, Pdgfrβ marks a specialized subset of WAT SV cells, fibro-inflammatory progenitors (FIPs), that are functionally distinct from APCs.[44] For instance, FIPs are non-adipogenic and exert a pro-inflammatory response upon activation and HFD administration.[20,44,45] Yet, our study does not directly assess Pdgfrβ-FIP activity, instead focusing on Pdgfrβ as a likely early adipose lineage specifier. A possible area of interest would be to assess if Pdgfrβ-deficient FIPs have altered lineage trajectory or functionality in response to HFD activation. Going forward, a key challenge will be to evaluate when Pdgfrβ signaling is required for adult APC lineage commitment and FIP function. This includes identifying Pdgfrβ required embryonic time points and the primordial niche of adult APCs prior to tissue infiltration.[9] Furthermore, understanding how obesity influences lineage (APCs and FIPs) progression and trajectory will aid in exposing molecular mediators of adipose-inflammatory functions.

Pdgfrβ appears to be among a select group of genes required for maintaining APC lineage commitment.[1,2] The absence of Pdgfrβ results in an adipose-to-macrophage lineage conversion, slowing WAT growth and fostering chronic low-grade inflammatory cues. In addition to Pdgfrβ, our findings support the notion that Pparγ marks embryonic adult APCs.[14] Although Pparγ is notorious for inducing adipogenesis and lipid storage, its role in APCs is less understood.[46,47] Previous efforts have focused on Pparγ's role in APC proliferation and niche interaction, but the Pparγ-driven molecular underpinnings of APC lineage restriction remain unknown.[14] Recent efforts by Teruel and colleagues have shown that Pparγ expression oscillates within APCs prior to differentiation, suggesting a role for Pparγ prior to and initiating adipogenesis.[48,49] Also, Pparγ can be post-translationally modified.[50] For example, Pparγ can be phosphorylated at serine 112, blocking its transcriptional activity and halting adipogenesis.[40,41] However, the implications of Pparγ phosphorylation on gene regulation in APC biology are still unfolding.[45] It is notable that the activation of Pdgfrβ can promote Pparγ phosphorylation at serine 112, while stimulating APC proliferation. Interestingly, imatinib, a Pdgfrβ pharmacological target, can reduce Pparγ phosphorylation, suggesting a potential clinical entry point to control adipocyte number and health.[45]

Adipose tissue dysfunction is accompanied by immunologic cellular composition changes leading to a proinflammatory response.[24] In agreement, we observe low immunological activation under control NCD conditions, HFD administration induces dramatic immunological composition remodeling.[24,51] Under Pdgfrβ^{AT}KO$^{E10.5}$ deletion, we observe elevated immunological conditions that become heightened with tissue dysfunction. Yet, our studies did not decipher differences in immunological cell composition nor their activation, accrual, and regulation in response to Pdgfrβ^{AT}KO$^{E10.5}$ deletion. Going forward, it would be of interest if diet-induced obesity influences APC lineage decisions, similar to Pdgfrβ ablation.[52] Notably, our limited examination of HFD's impact on E10.5 APC lineage fidelity suggests this may not occur in adult WATs. We speculate that these restrictions are potential roadblocks to triggering the wrong stem cell fate. A deeper investigation into APC lineage regulation and confinement could provide insight into inflammatory cues or fibrotic tissue replacement. What is more, aberrant developmental and adult signals can drive imbalances in progenitor cell abundance, lineage decision, and target tissue organogenesis and function.[44,53] For example, parental obesity increases the risk of childhood and adult obesity and its associated metabolic disorders, such as cardiometabolic disease.[54] However, the interplay between diet, genetics, and the environment and its influence on the adipose lineage remains vague. Nonetheless, Pdgfrβ appears to act as an embryonic molecular rheostat of the APC lineage identity to coordinate adult WAT expansion and accumulation.

Limitations of the study

Tissue lineage determination and specification are critical for tissue development, homeostasis, and regeneration. Adipose tissue lineage fidelity is key to preserving WAT growth and expansion, especially under obesogenic conditions. Moreover, elucidating the sex-dependent regulatory features of the adipose lineage trajectory are key to understanding differential metabolic responses and WAT function. While our

work provides insight into the molecular regulation and determination of the adipose lineage, these studies were conducted using male mice. Although, these initial observations provide a working model for adipose lineage specification and tissue function, future research should focus on the sex-dependent regulation of adipose tissue development and homeostasis to coordinate systemic metabolism.

STAR★METHODS

Detailed methods are provided in the online version of this paper and include the following:

- KEY RESOURCES TABLE
- RESOURCE AVAILABILITY
  - Lead contact
  - Materials availability
  - Data and code availability
- EXPERIMENTAL MODEL AND STUDY PARTICIPANT DETAILS
  - Animal studies
- METHOD DETAILS
  - Food intake analysis
  - Body composition analysis
  - High-fat diet
  - BrdU injection
  - Glucose tolerance test
  - Blood chemistry
  - Adipose SV cell isolation
  - Adipogenesis
  - Lipid staining
  - SVP isolation and quantification
  - Flow cytometry
  - RNA isolation and qPCR
  - Histological analysis
  - Immunoblotting
- QUANTIFICATION AND STATISTICAL ANALYSIS

SUPPLEMENTAL INFORMATION

Supplemental information can be found online at https://doi.org/10.1016/j.isci.2023.108682.

ACKNOWLEDGMENTS

The authors thank Dr. Benjamin M. Steiner and Heather Roman for technical assistance and aid in collecting preliminary observations. The authors thank the Cornell Biotechnology Resources Center Flow Cytometric Core Facility and the Center of Animal Resources and Education for excellent assistance with experimental collection and mouse husbandry, respectively. This work was supported by Cornell University internal funds and NIDDK awards K01 DK109027 and R03 DK122193 to D.C.B. and D.C.B is supported by an NIH-NIDDK award R01 DK132264-01.

AUTHOR CONTRIBUTIONS

Conceptualization, A.M.B., Y.J., and D.C.B.; Methodology, A.M.B., Y.J., and D.C.B.; investigation, A.M.B., D.L., Y.J., and D.C.B.; writing – original draft, A.M.B., D.L., and D.C.B.; writing – review and editing, A.M.B., D.L., Y.J., and D.C.B.; funding acquisition, D.C.B.; resources, D.C.B.; supervision, D.C.B.

DECLARATION OF INTERESTS

The authors declare no competing interests.

INCLUSION AND DIVERSITY

One or more of the authors of this paper self-identifies as a member of the LGBTQIA+ community.

Received: September 6, 2023
Revised: October 31, 2023
Accepted: December 5, 2023
Published: December 12, 2023

REFERENCES

1. Berry, D.C., Stenesen, D., Zeve, D., and Graff, J.M. (2013). The developmental origins of adipose tissue. Development *140*, 3939–3949.
2. Gesta, S., Tseng, Y.H., and Kahn, C.R. (2007). Developmental origin of fat: tracking obesity to its source. Cell *131*, 242–256. S0092-8674(07)01272-X [pii].
3. Wang, Q.A., Tao, C., Gupta, R.K., and Scherer, P.E. (2013). Tracking adipogenesis during white adipose tissue development, expansion and regeneration. Nat. Med. *19*, 1338–1344.
4. Jeffery, E., Wing, A., Holtrup, B., Sebo, Z., Kaplan, J.L., Saavedra-Peña, R., Church, C.D., Colman, L., Berry, R., and Rodeheffer, M.S. (2016). The Adipose Tissue Microenvironment Regulates Depot-Specific Adipogenesis in Obesity. Cell Metabol. *24*, 142–150.
5. Rosen, E.D., and Spiegelman, B.M. (2014). What we talk about when we talk about fat. Cell *156*, 20–44.
6. Sakers, A., De Siqueira, M.K., Seale, P., and Villanueva, C.J. (2022). Adipose-tissue plasticity in health and disease. Cell *185*, 419–446.
7. Scheja, L., and Heeren, J. (2019). The endocrine function of adipose tissues in health and cardiometabolic disease. Nat. Rev. Endocrinol. *15*, 507–524.
8. Vishvanath, L., and Gupta, R.K. (2019). Contribution of adipogenesis to healthy adipose tissue expansion in obesity. J. Clin. Invest. *129*, 4022–4031.
9. Berry, D.C., Jiang, Y., and Graff, J.M. (2016). Emerging Roles of Adipose Progenitor Cells in Tissue Development, Homeostasis, Expansion and Thermogenesis. Trends Endocrinol. Metabol. *27*, 574–585.
10. Merrick, D., Sakers, A., Irgebay, Z., Okada, C., Calvert, C., Morley, M.P., Percec, I., and Seale, P. (2019). Identification of a mesenchymal progenitor cell hierarchy in adipose tissue. Science *364*.
11. Schwalie, P.C., Dong, H., Zachara, M., Russeil, J., Alpern, D., Akchiche, N., Caprara, C., Sun, W., Schlaudraff, K.U., Soldati, G., et al. (2018). A stromal cell population that inhibits adipogenesis in mammalian fat depots. Nature *559*, 103–108.
12. Sanchez-Gurmaches, J., and Guertin, D.A. (2014). Adipocytes arise from multiple lineages that are heterogeneously and dynamically distributed. Nat. Commun. *5*, 4099.
13. Berry, D.C., Jiang, Y., and Graff, J.M. (2016). Mouse strains to study cold-inducible beige progenitors and beige adipocyte formation and function. Nat. Commun. *7*, 10184.
14. Jiang, Y., Berry, D.C., Tang, W., and Graff, J.M. (2014). Independent stem cell lineages regulate adipose organogenesis and adipose homeostasis. Cell Rep. *9*, 1007–1022.
15. Tang, W., Zeve, D., Suh, J.M., Bosnakovski, D., Kyba, M., Hammer, R.E., Tallquist, M.D., and Graff, J.M. (2008). White fat progenitor cells reside in the adipose vasculature. Science *322*, 583–586. 1156232 [pii].
16. Lee, Y.H., Petkova, A.P., Mottillo, E.P., and Granneman, J.G. (2012). In vivo identification of bipotential adipocyte progenitors recruited by beta3-adrenoceptor activation and high-fat feeding. Cell Metabol. *15*, 480–491.
17. Gupta, R.K., Mepani, R.J., Kleiner, S., Lo, J.C., Khandekar, M.J., Cohen, P., Frontini, A., Bhowmick, D.C., Ye, L., Cinti, S., and Spiegelman, B.M. (2012). Zfp423 expression identifies committed preadipocytes and localizes to adipose endothelial and perivascular cells. Cell Metabol. *15*, 230–239. S1550-4131(12)00014-9 [pii].
18. Fuchs, E., and Blau, H.M. (2020). Tissue Stem Cells: Architects of Their Niches. Cell Stem Cell *27*, 532–556.
19. Jiang, Y., Berry, D.C., Jo, A., Tang, W., Arpke, R.W., Kyba, M., and Graff, J.M. (2017). A PPARgamma transcriptional cascade directs adipose progenitor cell-niche interaction and niche expansion. Nat. Commun. *8*, 15926.
20. Zhang, Q., Shan, B., Guo, L., Shao, M., Vishvanath, L., Elmquist, G., Xu, L., and Gupta, R.K. (2022). Distinct functional properties of murine perinatal and adult adipose progenitor subpopulations. Nat. Metab. *4*, 1055–1070.
21. Hudak, C.S., Gulyaeva, O., Wang, Y., Park, S.M., Lee, L., Kang, C., and Sul, H.S. (2014). Pref-1 marks very early mesenchymal precursors required for adipose tissue development and expansion. Cell Rep. *8*, 678–687.
22. Tumbar, T., Guasch, G., Greco, V., Blanpain, C., Lowry, W.E., Rendl, M., and Fuchs, E. (2004). Defining the epithelial stem cell niche in skin. Science *303*, 359–363.
23. Sun, K., Tordjman, J., Clément, K., and Scherer, P.E. (2013). Fibrosis and adipose tissue dysfunction. Cell Metabol. *18*, 470–477.
24. Reilly, S.M., and Saltiel, A.R. (2017). Adapting to obesity with adipose tissue inflammation. Nat. Rev. Endocrinol. *13*, 633–643.
25. Austyn, J.M., and Gordon, S. (1981). F4/80, a monoclonal antibody directed specifically against the mouse macrophage. Eur. J. Immunol. *11*, 805–815.
26. Stefan, N. (2020). Causes, consequences, and treatment of metabolically unhealthy fat distribution. Lancet Diabetes Endocrinol. *8*, 616–627.
27. Zeve, D., Seo, J., Suh, J.M., Stenesen, D., Tang, W., Berglund, E.D., Wan, Y., Williams, L.J., Lim, A., Martinez, M.J., et al. (2012). Wnt signaling activation in adipose progenitors promotes insulin-independent muscle glucose uptake. Cell Metabol. *15*, 492–504. S1550-4131(12)00106-4 [pii].
28. Soriano, P. (1999). Generalized lacZ expression with the ROSA26 Cre reporter strain. Nat. Genet. *21*, 70–71.
29. Ho, M.K., and Springer, T.A. (1982). Mac-2, a novel 32,000 Mr mouse macrophage subpopulation-specific antigen defined by monoclonal antibodies. J. Immunol. *128*, 1221–1228.
30. Wynn, T.A., Chawla, A., and Pollard, J.W. (2013). Macrophage biology in development, homeostasis and disease. Nature *496*, 445–455.
31. Charrière, G., Cousin, B., Arnaud, E., André, M., Bacou, F., Pénicaud, L., and Casteilla, L. (2003). Preadipocyte Conversion to Macrophage EVIDENCE OF PLASTICITY. J. Biol. Chem. *278*, 9850–9855.
32. Lackey, D.E., and Olefsky, J.M. (2016). Regulation of metabolism by the innate immune system. Nat. Rev. Endocrinol. *12*, 15–28.
33. Olson, L.E., and Soriano, P. (2011). PDGFRbeta signaling regulates mural cell plasticity and inhibits fat development. Dev. Cell *20*, 815–826.
34. Vishvanath, L., MacPherson, K.A., Hepler, C., Wang, Q.A., Shao, M., Spurgin, S.B., Wang, M.Y., Kusminski, C.M., Morley, T.S., and Gupta, R.K. (2016). Pdgfrbeta+ Mural Preadipocytes Contribute to Adipocyte Hyperplasia Induced by High-Fat-Diet Feeding and Prolonged Cold Exposure in Adult Mice. Cell Metabol. *23*, 350–359.
35. Jeffery, E., Church, C.D., Holtrup, B., Colman, L., and Rodeheffer, M.S. (2015). Rapid depot-specific activation of adipocyte precursor cells at the onset of obesity. Nat. Cell Biol. *17*, 376–385.
36. He, C., Medley, S.C., Kim, J., Sun, C., Kwon, H.R., Sakashita, H., Pincu, Y., Yao, L., Eppard, D., Dai, B., et al. (2017). STAT1 modulates tissue wasting or overgrowth downstream from PDGFRbeta. Genes Dev. *31*, 1666–1678.
37. He, C., Medley, S.C., Hu, T., Hinsdale, M.E., Lupu, F., Virmani, R., and Olson, L.E. (2015). PDGFR beta signalling regulates local inflammation and synergizes with hypercholesterolaemia to promote atherosclerosis. Nat. Commun. *6*, 7770. ARTN 7770.
38. Benvie, A.M., Lee, D., Steiner, B.M., Xue, S., Jiang, Y., and Berry, D.C. (2023). Age-dependent Pdgfrbeta signaling drives adipocyte progenitor dysfunction to alter the beige adipogenic niche in male mice. Nat. Commun. *14*, 1806.
39. Heldin, C.H., and Westermark, B. (1999). Mechanism of action and in vivo role of platelet-derived growth factor. Physiol. Rev. *79*, 1283–1316.
40. Adams, M., Reginato, M.J., Shao, D., Lazar, M.A., and Chatterjee, V.K. (1997). Transcriptional activation by peroxisome proliferator-activated receptor gamma is inhibited by phosphorylation at a consensus mitogen-activated protein kinase site. J. Biol. Chem. *272*, 5128–5132.
41. Hu, E., Kim, J.B., Sarraf, P., and Spiegelman, B.M. (1996). Inhibition of adipogenesis through MAP kinase-mediated phosphorylation of PPARgamma. Science *274*, 2100–2103.
42. Young, P.R., McLaughlin, M.M., Kumar, S., Kassis, S., Doyle, M.L., McNulty, D., Gallagher, T.F., Fisher, S., McDonnell, P.C., Carr, S.A., et al. (1997). Pyridinyl imidazole inhibitors of p38 mitogen-activated protein kinase bind in the ATP site. J. Biol. Chem. *272*, 12116–12121.
43. Gao, Z., Daquinag, A.C., Su, F., Snyder, B., and Kolonin, M.G. (2018). PDGFRalpha/PDGFRbeta signaling balance modulates progenitor cell differentiation into white and beige adipocytes. Development *145*.
44. Shan, B., Shao, M., Zhang, Q., Hepler, C., Paschoal, V.A., Barnes, S.D., Vishvanath, L., An, Y.A., Jia, L., Malladi, V.S., et al. (2020). Perivascular mesenchymal cells control adipose-tissue macrophage accrual in obesity. Nat. Metab. *2*, 1332–1349.
45. Shao, M., Hepler, C., Zhang, Q., Shan, B., Vishvanath, L., Henry, G.H., Zhao, S., An, Y.A., Wu, Y., Strand, D.W., and Gupta, R.K. (2021). Pathologic HIF1alpha signaling drives adipose progenitor dysfunction in obesity. Cell Stem Cell *28*, 685–701.e7.
46. Tontonoz, P., Hu, E., and Spiegelman, B.M. (1994). Stimulation of adipogenesis in fibroblasts by PPAR gamma 2, a lipid-activated transcription factor. Cell *79*, 1147–1156. 0092-8674(94)90006-X [pii].

47. Chawla, A., Schwarz, E.J., Dimaculangan, D.D., and Lazar, M.A. (1994). Peroxisome proliferator-activated receptor (PPAR) gamma: adipose-predominant expression and induction early in adipocyte differentiation. Endocrinology *135*, 798–800.
48. Zhao, M.L., Rabiee, A., Kovary, K.M., Bahrami-Nejad, Z., Taylor, B., and Teruel, M.N. (2020). Molecular Competition in G1 Controls When Cells Simultaneously Commit to Terminally Differentiate and Exit the Cell Cycle. Cell Rep. *31*, 107769.
49. Bahrami-Nejad, Z., Zhao, M.L., Tholen, S., Hunerdosse, D., Tkach, K.E., van Schie, S., Chung, M., and Teruel, M.N. (2018). A Transcriptional Circuit Filters Oscillating Circadian Hormonal Inputs to Regulate Fat Cell Differentiation. Cell Metabol. *27*, 854–868.e8.
50. Tontonoz, P., and Spiegelman, B.M. (2008). Fat and beyond: the diverse biology of PPARgamma. Annu. Rev. Biochem. *77*, 289–312.
51. Wernstedt Asterholm, I., Tao, C., Morley, T.S., Wang, Q.A., Delgado-Lopez, F., Wang, Z.V., and Scherer, P.E. (2014). Adipocyte inflammation is essential for healthy adipose tissue expansion and remodeling. Cell Metabol. *20*, 103–118.
52. Ge, Y., Gomez, N.C., Adam, R.C., Nikolova, M., Yang, H., Verma, A., Lu, C.P.J., Polak, L., Yuan, S., Elemento, O., and Fuchs, E. (2017). Stem Cell Lineage Infidelity Drives Wound Repair and Cancer. Cell *169*, 636–650.e14.
53. Ghaben, A.L., and Scherer, P.E. (2019). Adipogenesis and metabolic health. Nat. Rev. Mol. Cell Biol. *20*, 242–258.
54. Godfrey, K.M., Reynolds, R.M., Prescott, S.L., Nyirenda, M., Jaddoe, V.W.V., Eriksson, J.G., and Broekman, B.F.P. (2017). Influence of maternal obesity on the long-term health of offspring. Lancet Diabetes Endocrinol. *5*, 53–64.
55. Perl, A.K.T., Wert, S.E., Nagy, A., Lobe, C.G., and Whitsett, J.A. (2002). Early restriction of peripheral and proximal cell lineages during formation of the lung. Proc. Natl. Acad. Sci. USA *99*, 10482–10487.
56. Schmahl, J., Rizzolo, K., and Soriano, P. (2008). The PDGF signaling pathway controls multiple steroid-producing lineages. Genes Dev. *22*, 3255–3267.
57. Madisen, L., Zwingman, T.A., Sunkin, S.M., Oh, S.W., Zariwala, H.A., Gu, H., Ng, L.L., Palmiter, R.D., Hawrylycz, M.J., Jones, A.R., et al. (2010). A robust and high-throughput Cre reporting and characterization system for the whole mouse brain. Nat. Neurosci. *13*, 133–140.
58. Tang, W., Zeve, D., Seo, J., Jo, A.Y., and Graff, J.M. (2011). Thiazolidinediones regulate adipose lineage dynamics. Cell Metabol. *14*, 116–122. S1550-4131(11)00218-X [pii].
59. Hausman, D.B., Park, H.J., and Hausman, G.J. (2008). Isolation and culture of preadipocytes from rodent white adipose tissue. Methods Mol. Biol. *456*, 201–219.
60. Berry, D.C., and Noy, N. (2009). All-trans-retinoic acid represses obesity and insulin resistance by activating both peroxisome proliferation-activated receptor beta/delta and retinoic acid receptor. Mol. Cell Biol. *29*, 3286–3296.
61. Berry, D.C., Soltanian, H., and Noy, N. (2010). Repression of cellular retinoic acid-binding protein II during adipocyte differentiation. J. Biol. Chem. *285*, 15324–15332.

STAR★METHODS

KEY RESOURCES TABLE

REAGENT or RESOURCE	SOURCE	IDENTIFIER
Antibodies		
Anti-mouse CD45 antibody	Biolegend	Cat#103151; RRID: AB_2565884
Anti-mouse Brdu antibody	Invitrogen	Cat#48-5071-41; RRID:AB_2574065
Anti-mouse CD68 antibody	Biolegend	Cat#137003; RRID: AB_2044001
Phosphorylated Stat1	Cell Signaling	Cat#9167S; RRID:AB_561284
Phosphorylated P38	Cell Signaling	Cat#4511S; RRID:AB_2139682
Cy5-Donkey Anti-Rabbit	Jackson Immunoresearch	Cat#711-005-152; RRID:AB_2340585
guinea pig anti-perilipin antibody	Fitzgerald	Cat#20R-PP004; RRID:AB_1288416
rabbit anti-DsRed antibody	Takara	Cat#632496; RRID:AB_10013483
mouse anti-alpha-smooth muscle actin antibody	NovusBio	Cat#2-34760V; RRID:AB_2923381
rat anti- Mac 2 antibody	Cedarlane	Cat#CL8942AP; RRID:AB_10060357
rat anti-F4/80 antibody	R&D Systems	Cat#MAB5580-SP; RRID:AB_2098328
Cy5 donkey anti-guinea pig	Invitrogen	Cat#A-21450; RRID:AB_141882
Texas red donkey anti-rabbit	Invitrogen	Cat#A10042; RRID:AB_2534017
488 donkey anti-rat	Invitrogen	Cat#A-21208; RRID:AB_2535794
Phosphorylated Ppargamma (Ser112)	EMD Millipore	Cat#04-816-I; RRID: AB_10563102
Phosphorylated Pdgfrβ (Y1009)	Cell Signaling	Cat#3124S; RRID:AB_823455
GAPDH	Cell Signaling	Cat#2118S; RRID: AB_561053
Beta-Tubulin	Cell Signaling	Cat#15115; RRID: AB_2798712
Donkey anti-rabbit IgG (H+L) Cross-Adsorbed Secondary Antibody, HRP	Invitrogen	Cat#31458; RRID: AB_228213
Chemicals, peptides, and recombinant proteins		
TRIzol Reagent	ambion	Cat#15596018
Phosphate buffered saline powder, pH 7.4	Sigma-Aldrich	Cat#1003015902
10% Buffered Formalin Phosphate	Fisherchemical	Cat#SF100-4
Gill 2 Hematoxlyin	Epredia	Cat#72511
Bluing Reagent	thermoscientific	Cat#7301
High Def	StatLab	Cat#SL103
Eosin-Y	thermoScientific	Cat#71225
Xylene Substitute	Epredia	Cat#9990505
R-Buffer A, 10X, pH 6	Electron Microscopy Sciences	Cat#62706-10
Triton X-100, 10% solution, peroxide-free	amresco	Cat#M236-10ML
DMEM/F12(1:1)(1x)	gibco	Cat#11320-033
Pen Strep	gibco	Cat#15140-122
TRIS-Tricine-SDS Running Buffer (10X)	Bio Rad	Cat#1610744
10X Tris/Glycine Buffer	Bio Rad	Cat#1610771
Precision Plus Protein Dual Color Standards	Bio Rad	Cat#1610374
HCS LipidTOXTM Green neutral lipid stain	Invitrogen	Cat#H34475
Doxycycline diet (600 mg/Kg)	BioServe	Cat#F4107

(*Continued on next page*)

Continued

REAGENT or RESOURCE	SOURCE	IDENTIFIER
Brdu	BD Biosciences	Cat#51-2354AK
Recombinant Pdgf-BB	VWR	Cat#10780-770
SB203580	Cayman Chemicals	Cat#13067
Critical commercial assays		
Triglyceride Quantification Colorometric/Fluorometric Kit	Sigma-Aldrich	Cat#MAK266
UltraSensitive Insulin ELISA Kit	Alpco	Cat#80-INSUMSU-E01
Quantikine ELISA Mouse Adiponectin/Acrp30	R&D Systems	Cat#MRP30
High Capacity cDNA Reverse Transcription Kit	applied biosystems	Cat#4368813
Pierce BCA Protein Assay Kit	thermoscientific	Cat#23225
PowerUp SYBR Green Master Mix	Applied Biosystems	Cat#A25742
SuperSignalTM West Pico PLUS Chemiluminescent Substrate	thermoscientific	Cat#34580
Vectastain Universal Quick Kit	Vector Labs	Cat#PK-8800
Vectastain ABC Kit	Vector Labs	Cat#PK-4000
Peroxidase Substrate Kit Vectastain	Vector Labs	Cat#SK-4100
Experimental models: Organisms/strains		
Mouse: R26-tdtomato: B6.Cg-Gt(ROSA) 26Sortm14(CAG-tdTomato)Hze/J	The Jackson Laboratory	JAX: 007914; RRID:IMSR_JAX:007914
Mouse: Pparg-tTA: B6;129-*Pparg*$^{tm1.1(tTA)Jmgr}$/J	The Jackson Laboratory	JAX: 024755; RRID:IMSR_JAX:024755
Mouse: TRE-Cre: B6.Cg-Tg(tetO-cre)1Jaw/J	The Jackson Laboratory	JAX: 006234; RRID:IMSR_JAX:006234
Mouse: Pdgfrβ$^{fl/fl}$: 129S/SvJae-*Pdgfrβ*^{tm11Sor}/J	The Jackson Laboratory	JAX: 01097; RRID:IMSR_JAX:010977
Software and algorithms		
Attune Cytometric Software	Invitrogen	Version 5.3.2415.0
BD FACSDiva Software	BD Biosciences	Version 9.4; RRID:SCR_001456
Fiji - Image J Software	ImageJ2	https://imagej.net/; RRID:SCR_003070
FlowJo Software	FlowJo, LLC	Version 10; RRID:SCR_008520
BioRender	BioRender	http://biorender.com/; RRID:SCR_018361

RESOURCE AVAILABILITY

Lead contact

Further information and requests for resources and reagents should be directed to and will be fulfilled by the lead contact, Daniel C. Berry (dcb37@cornell.edu)

Materials availability

This study did not generate unique reagents.

Data and code availability

- Data. All data reported in this paper will be shared by the lead contact upon request.
- Code. This paper does not report original code.
- Any additional information required concerning the data reported in this paper is available from the lead contact upon request.

EXPERIMENTAL MODEL AND STUDY PARTICIPANT DETAILS

Animal studies

All animal experiments were performed according to procedures approved by the Cornell University Institutional Animal Care and Use Committee under the auspices of protocol number 2017-0063. AdipoTrak mice were previously[15] created using the following genetic models: Pparγ-tTA (stock #024755 Jackson Laboratories), TRE-Cre (tetO-cre; stock #006234; Jackson Laboratories)[55] and TRE-H2B-GFP (generously provided by Dr. Tudorita Tumbar).[22] Offspring were intercrossed for six generations prior to experimentation and were maintained on mixed C57BL/6J-129SV background. AdipoTrak mice were combined with Pdgfrβ$^{fl/fl}$ conditional mouse model purchased from Jackson laboratories (stock #010977).[56] Mice were then crossed with the Rosa26-^{tdtomato} (stock #007914).[57] Mice were maintained in a vivarium on a 14:10-hour light/dark cycle with free access to food (Chow diet: Teklad LM-485 Mouse/Rat Sterilizable Diet) and water. For doxycycline experiments, time mated plugged dams were administered doxycycline diet (600 mg/kg, Bio Serv Cat# F4107).[14] Dams and subsequent offspring were maintained on Dox diet as denoted in Figures. All animal experiments were performed on male mice at ages and developmental times denoted within figure legends. We utilized male mice due to the lack of adipose lineage characterization, progression, and trajectory in female AdipoTrak mice.[14,19] All experiments were performed on 3 or more mice per cohort and performed at least twice. Animals were euthanized by carbon dioxide asphyxiation and cervical dislocation was performed as a secondary euthanasia procedure.

METHOD DETAILS

Food intake analysis

To monitor food intake, mice were individually housed with a predetermined (~100 g) amount of food. Food weight was recorded every 24-hour cycle up to five days. Bedding was analyzed for excess food deposits and such mice were excluded from data collection.

Body composition analysis

A nuclear magnetic resonance (NMR) Bruker Minispec LF65 benchtop body composition analyzer was used.

High-fat diet

Control^{AT} and Pdgfrβ^{AT}KO male mice were fed a high fat diet (Research diets; D12492; 60% fat) for 12 weeks. Prior to and at the completion of the diet, body composition and body weight were collected.

BrdU injection

Control^{AT} and Pdgfrβ^{AT}KO male mice were administered one dose of Brdu (100 mg/kg; BD Biosciences 51-2354AK) dissolved in sterile 1X PBS for five consecutive days by intraperitoneal injection.[58]

Glucose tolerance test

Mice were fasted for six-hours prior to glucose tolerance test. Prior to fasting, a small tail snip was made, and baseline glucose measurements were determined. Mice were then i.p injected with glucose (1.25g/kg; Sigma G8270, dissolved in sterile water). Blood glucose levels were measured at times 0 (fasted), 15, 30, 45, 60, 90- and 120-minutes post injection with a Bayer Contour glucometer and strips.[19]

Blood chemistry

Blood was collected via heart puncture with non-heparinized needles. Collected blood was allowed to coagulate for 2 hours at room temperature. Samples were centrifuged at 7500 rpm for 5 minutes. Serum was collected, aliquoted, and frozen at -80°C. *Insulin ELISA:* To determine serum insulin levels, the mouse UltraSensitive Insulin ELISA Kit (Ref: 80-INSUMSU-E01) from Alpco was used as per the manufactures protocol. Serum samples were diluted 1:16 prior to measurement. *Adiponectin ELISA:* To determine adiponectin serum levels, the Quantikine ELISA Mouse Adiponectin/Acrp30 (R&D Systems, Catalog: MRP30) was used, following the manufacturer's protocol. Serum was diluted 1:2000 prior to measurement. *Triglyceride Assay:* To determine serum triglyceride levels, the Triglyceride Quantification Colorimetric/Fluorometric Kit from Millipore-Sigma (Sigma-Aldrich Catalog: MAK266) was used, following the manufacturer's protocol at 1:25 dilution.

Adipose SV cell isolation

A pair of inguinal adipose depots from a single mouse were minced and placed in 10 ml of isolation buffer (0.1 M HEPES, 0.12 M NaCl, 50 mM KCl, 5 mM D-glucose, 1.5% BSA, 1 mM $CaCl_2$) supplemented with collagenase type I (10,000 units: LS004194) and incubated in a 37°C incubator with gentle agitation for ~1 hour.[59] Serum free Dulbecco's Modified Eagle's Medium Nutrient Mixture F-12 Ham (Sigma, cat. no. D8900 and D6421) (DMEM/F12) media was added to the digested tissue and strained through a 100 μm cell strainer. Samples were spun at 1250 rpm for 10 minutes. After supernatant removal, the pellet was resuspended in 10 ml of erythrocyte lysis buffer (155 mM NH_4Cl, 10 mM $KHCO_3$, 0.1 mM EDTA) and gently vortexed to resuspend pellet. After a 5-minute incubation period, growth media (DMEM/F12 supplemented with 10% fetal bovine serum (FBS)) was added, mixed, and strained through a 40 μm cell strainer. Samples were then spun at 1250 rpm for 5 minutes.[59] For cell culture experiments, the cell pellet was resuspended in growth media and plated. After 12 hours, growth media was removed and replenished. For *in vitro* doxycycline treatments, cultures were administered 10 ug of doxycycline daily.

Adipogenesis

Isolated SV cells were grown to confluency. To induce white adipogenesis, confluent cells were treated with white adipogenic media one (DMEM/F12 supplemented with 5% FBS 10 μg/ml insulin, 1μM Dexamethasone, and 250 μM 3-Isobutyl-1-methylxanthine) for 72 hours. After 72 hours, white adipogenic media one was removed and replaced with white adipogenic media two (DMEM/F12 supplemented with 10% FBS 10 ug/ml insulin). Adipogenesis was assessed by LipidTox™ staining and mRNA expression.[60,61]

Lipid staining

At the end of adipogenesis, media was aspirated, and adipocytes were fixed with 4% paraformaldehyde for 45 minutes. Adipocytes were washed 3X with 1X TBS for 5-minutes. Adipocytes were permeabilized using 0.3%TritonX-100 in 1X TBS for 30 minutes. Adipocytes were washed 3X with 1X TBS for five minutes/wash. Adipocytes were incubated with HSC LipidTox-deep red or green (1/1000 in 1X TBS) for 45 minutes rocking in the dark. Adipocytes were washed twice with 1X TBS for five minutes/wash. Adipocytes were then stained with Hoechst (1 μg/ml in 1X TBS) for 10 minutes. Adipocytes were washed twice with 1X TBS for five minutes/wash. Fluorescent images were collected on a Leica DMi8 inverted microscope system.

SVP isolation and quantification

WATs were isolated and digested as described in the SVF isolation. The SVP tubes that remained on the 100 μm mesh were collected into growth media. SVPs were pelleted at 500 rpm for 10 minutes. Supernatant was aspirated and SVPs were cultured on microscope coverslips that were precoated with 1% fibronectin (Sigma: item no.: F1141). SVPs were imaged 12-16 hours later for GFP or tdTomato occupancy. We quantified 10 SVPs/mouse for 3 mice/group. SVP distance was measured using the Leica Application Suite X Microscope software.[15,19,38]

Flow cytometry

The iWAT SVF was isolated as above and resuspended in 1X PBS along with blue-fluorescent reactive dye. Cells were then pelleted (1250 rpm for 10 minutes), resuspended in 0.3-0.5 ml of FACS buffer (2.5% horse serum; 2 mM EDTA in 1X PBS with 1X protease/phosphatase inhibitor cocktail) and filtered through a 5 ml cell-strainer capped FACS tube (BD Falcon). Cell sorting was performed on BD Biosciences FACSAria Fusion, or cells were analyzed on a Thermo-Fisher Attune NxT cytometry. Viable cells were gated from the blue-fluorescent reactive dye negative population followed by singlet forward and side scatter pattern. A negative control sample was used to establish negative versus positive fluorescent signal. Cells were analyzed for GFP or RFP positivity. Alternatively, fixed cells were stained for CD45 (1:400 Biolegend 103151), Brdu (1:200; invitrogen 48-5071-41), or CD68 (1:200; Biolegend 137003). For phosphorylated Stat1 or p38 analysis, cells were fixed with 4% PFA for 1 hour at room temperature. Subsequently, cells were washed with 1X TBS and permeabilized for 30 minutes at room temperature with 0.3%TritonX-100 in 1X TBS. Cells were blocked with 5% donkey serum in 1X TBS for 30-minutes and incubated with primary antibody in 1X TBS with 5% donkey serum overnight at 4°C. Primary antibodies used were phosphorylated Stat1 (1:200; 9167S Cell Signaling) or phosphorylated p38 (1:200; 4511S Cell Signaling). After washing, secondary antibodies were applied for 2 hours at room temperature in the dark, then analyzed. Secondary antibodies used were Cy5 donkey anti-rabbit (1:200; Jackson ImmunoResearch).

RNA isolation and qPCR

For tissues, ~150-300 mg of iWAT or gWAT, from one mouse, was placed into Precellys tubes containing ceramic beads and 1 ml of TRIzol (Ambion 15596019). Tissues were homogenized in a Precellys 24 homogenizer using the following the settings: 3 pulses at 4500 rpm for 30 seconds with a 30 second rest between pulses with a final rest of 4 minutes. For cells, TRIzol was directly added to culture dishes and mechanically disrupted. RNA was extracted using the standard chloroform extraction and isopropanol precipitation method. RNA concentration and quality were determined using a TECAN infinite F-nano^{+} spectrophotometer. 1 μg of RNA was converted to cDNA using the high-capacity RNA to cDNA kit (Life Technologies #4368813). For qPCR, cDNA was diluted 1:10 and added to PowerUp™ SYBR™ Green Master Mix (Life Technologies A25742) along with denoted primers. qPCR analysis was performed on an Applied Biosystems QuantStudio™ 3 Real-Time PCR System using the DD-CT method compared to the internal control, Rn18s. Data points represent a biological replicate (single mouse or culture). Each data point was performed in a technical quadruplet. qPCR primer sequences can be found in Table S1 related to STAR Methods.

Histological analysis

Dissected tissues were immediately placed in 10% formalin (neutralized with 1X PBS) for 24 hours. Tissues were processed using Thermo Scientific™ STP 120 Spin Tissue Processor with the following conditions: Bucket 1: 50% ethanol (45 minutes); Bucket 2: 70% ethanol (45 minutes) Bucket 3: 80% ethanol (45 minutes); Bucket 4 and 5: 95% ethanol (45 minutes); Bucket 6 and 7: 100% ethanol (45 minutes); Bucket 8-10: Xylene Substitute (45 minutes); Bucket 11 and 12: paraffin (4 hours each). Tissues were embedded into cassettes using a Histostar™ embedding station. Blocks were refrigerated for at least 24 hours prior to sectioning. 8-12-micron tissue sections were generated using a HM-325 microtome using low profile blades. Sections were placed in a 40°C water bath and positioned on microscope slides. Slides were then baked overnight at 55 ºC prior to staining.

Hematoxylin and eosin (H&E) staining

Slides were rehydrated using the following protocol: xylene (3 minutes 3X), 100% reagent alcohol (1 minutes 2X); 95% reagent alcohol (1 min 2X); water (1 minutes). Slides were stained in hematoxylin and eosin (H&E) staining for 2:30 minutes and 10 repeated submerges, respectively. Slides were dehydrated in the reverse order of rehydration steps. Coverslips were mounted with Cytoseal 60 mounting media. Brightfield images were acquired using a Leica DMi8 inverted microscope system.

Immunohistochemistry (IHC) + immunofluorescent staining

Slides were rehydrated using the following protocol: xylene (3 minutes 3X), 100% reagent alcohol (1 minutes 2X); 95% reagent alcohol (1 min 2X); water (1 minutes). Antigen retrieval was performed using 1X Citrate Buffer, made from 10X stock (Electron Microscopy Sciences R-Buffer A, 10X, pH 6; Catalog: 62706-10), and placed into antigen retriever pressure cooker (EMS Catalog #62706) for 2 hours. Slides were permeabilized using 0.3%TritonX-100 in 1X TBS for 30 minutes and washed 3X in 1xTBS. Slides were blocked with 5% donkey serum in 1X TBS for 30-minutes and incubated with primary antibody in 1X TBS with 5% donkey/goat serum for either 1 hour at room temperature (21-23ºC) or overnight at 4°C. The following primary antibodies were used: guinea pig anti-perilipin (1:200; abcam: Fitzgerald 20R-PP004); rabbit anti-DsRed (1:100; Takara: 632496); mouse anti-alpha-smooth muscle actin (1:200; NovusBio 2-34760V); rat anti- Mac 2 (1:400; Cedarlane CL8942AP); rat anti-F4/80 (1:200; R&D Systems MAB5580-SP). Secondaries from Invitrogen were all used at 1:200 dilutions and incubated for 2 h at room temperature. The following secondary antibodies were used: Cy5 donkey anti-guinea pig, Texas red donkey anti-rabbit, or 488 donkey anti-rat. Slides were washed and stained with Hoechst (H3570; Life Technologies) (1 μg/ml in 1X TBS) for 10 minutes and cover slipped with Thermo Scientific™ Shandon™ Immu-Mount™ mounting media. Fluorescent images were collected on a Leica DMi8 inverted microscope system.

For IHC, peroxidase blocking was performed after primary antibody incubation using 0.3% hydrogen peroxide solution for 10 minutes at room temperature. Slides were washed 3X for 2 minutes with 0.05% PBS-Tween 20 and incubated in biotinylated secondary antibody (Vectastain Universal Quick Kit: PK-8800). After another wash, slides were exposed to ABC-Peroxidase Solution for 30 minutes at room temperature (Vectastain ABC Kit: PK-4000) and washed. Slides were then incubated in peroxidase substrate solution (Peroxidase Substrate Kit Vectastain: SK-4100) and washed then counterstained with hematoxylin for 3 minutes. Tissue sections were then rinsed with running water for 2-5 minutes, dehydrated in 95% ethanol (1min) and 100% ethanol (3 minutes 2X), and cleared in xylene (5 minutes 2X). Slides were mounted in Cryoseal 60 mounting media and brightfield images were collected under a Leica DMi8 inverted microscope.

Immunoblotting

The iWAT SVF was isolated as above, and samples were plated in 10 cm plates. Cultures were then grown and treated with either a vehicle (1X PBS 0.1% BSA), Pdgf-BB (25 ng/sample), SB203580 (1 uM/ sample) or the combination of Pdgf-BB and SB203580 for 15 minutes in serum free media prior to collection. Samples were then collected and lysed on ice using 200 μL RIPA Lysis Buffer. Lysed samples were then incubated for 30 min on ice, and spun for 15 minutes at 4 °C, and the supernatant collected. Standard curve and respective protein concentrations for samples were determined and calculated utilizing the protocol provided in the Pierce protein assay kit (Pierce™ BCA Protein Assay - ThermoScientific) and a TECAN infinite F-nano+ spectrophotometer to read absorbance. For sample preparation, the calculated volume of 100 μg of protein per sample was mixed at a 1:1 ratio of 2X SDS/DTT, then heated for 10 minutes at 100 °C. Prepared samples and protein ladder (Biorad 161-0374) were loaded into a 10% separating and stacking gel (Biorad 4561034). The gel was placed into a Mini-PROTEAN Tetra Electrophoresis Cell chamber (Biorad 1658004) suspended in 1x running buffer (Biorad 1610744) and ran at 90 V for ~2.5 hours. Protein was then transferred onto an immobilon PSQ PVDF membrane (Millipore ISEQ0005) in 1X transfer buffer (Biorad 1610771) for 1 hour at 100 V on ice. The resulting membrane was removed and washed with 1x TBS-0.1% Tween20 (TBS-T) 3X for 5 minutes on a rocker at room temperature. The membrane was then blocked with 5% BSA in 1X TBS-T for 1 hour at room temperature and washed. Prior to primary antibody addition, the membrane was cut depending on protein molecular weight. Primary antibody in 5% BSA in 1X TBS-T was added at 4 °C and incubated overnight. The primary antibodies used are as follows: rabbit anti-phosphorylated p38 (1:1000; Cell Signaling: 4511S); rabbit anti-phosphorylated Ppargamma (Ser112) (1:500; EMD Millipore 04-816-I); rabbit anti-phosphorylated Pdgfrβ (Y1009) (1:1000; Cell Signaling: 3124S); rabbit anti-GAPDH (1:1000; Cell Signaling: 2118); rabbit anti-beta-tubulin (1:1000; Cell Signaling: 15155S). Membranes were washed again and submerged in secondary antibody for 2 hours at room temperature, rocking (1:5,000; ThermoFisher Scientific: donkey anti-rabbit IgG (H + L) Cross-Adsorbed HRP 31458 in 5% BSA 1x TBS-T or 1:5000: ThermoFisher Scientific: donkey anti-rabbit IgG (H + L) Cross-Adsorbed HRP 31458 in 5% Milk 1x TBS-T. Subsequently, membranes were washed and submerged in a 1:1 solution of SuperSignal™ West Pico PLUS Chemiluminescent Substrate (ThermoScientific: 34580) for 3 minutes and developed utilizing a FlourChem E system (biotechne® proteinsimple).

QUANTIFICATION AND STATISTICAL ANALYSIS

Statistical significance was assessed by two-tailed Student's t-test for two-group comparisons. Two-way ANOVA was used for multiple group comparisons. Individual data points (sample size) are presented and plotted as means. Error bars are expressed as ± SEM. $P < 0.05$ was considered significant in all the experiments. The statistical parameters and the number of mice used per experiment are found in the figure legends. Mouse experiments were performed in biological duplicate or triplicate with at least three mice per group. Cell culture experiments were collected from three or four independent cultures for each sample. The flow cytometric analysis software, FlowJo version 10.8.1, BD

FACSDiva Software version 9.4, and Attune Cytometric Software 5.3.2415.0 was used to analyze cell populations and antibody staining. The Fiji ImageJ Adiposoft plugin was used to calculate adipocyte area; areas below 50 microns were omitted due to reliability. NIH Fiji Image J software was additionally used to quantify co-localization, fibrotic tissue area, and fluorescent positivity area. For image analysis, three random fields were assessed from at least three mice/cohort. The Leica Application Suite X Microscope software was used for image acquisition and analyses. Representative H&E staining and immunochemical images were obtained from at least 4-5 replicates per group. All graphs and statistical analysis were performed using GraphPad Prism 7-9 software. Excel was used for raw data collection, analysis, and quantification. Illustrations and experimental designs were created using PowerPoint and BioRender (https://www.biorender.com/).